Université de Montréal

Proteomics of mature extracellular Human coronavirus OC43

Par

Negar Joharinia

Département de microbiologie, infectiologie et immunologie

Faculté de médecine

Mémoire présenté à la Faculté de médecine
en vue de l'obtention du grade de Magister scientiae
en Microbiologie/ immunologie

Août 2023

© Negar Joharinia, 2023

Université de Montréal

Département de microbiologie, infectiologie et immunologie/ Faculté de médecine

---

Ce mémoire intitulé

Proteomics of mature extracellular Human coronavirus OC43

Présenté par

Negar Joharinia

A été évalué(e) par un jury composé des personnes suivantes

Guy Lemay
Président-rapporteur

Roger Lippé
Directeur de recherche

Soren Gantt
Membre du jury

Résumé

Le coronavirus humain OC43 (HCoV-OC43) est un bêta-coronavirus de la famille des *coronaviridae*. Contrairement au SRAS-CoV2, le HCoV-OC43 provoque une maladie des voies respiratoires supérieures. Cependant, en raison de leur proximité phylogénique étroite mais leur pathologie distincte, HCoV-OC43 est un substitut fort intéressant pour étudier et comparer les bêta-coronavirus. Comme tous les virus, ces derniers détournent les protéines de la machinerie cellulaire pour compléter leur cycle de vie. Les protéines cellulaires, en particulier celles incorporées dans les virions, sont particulièrement intéressantes puisqu'elles jouent souvent un rôle vital dans le cycle de vie du virus. Notre objectif est d'utiliser le pipeline protéomique que nous avons développé pour le HSV-1 afin de caractériser les protéines hôtes associées à des particules virales extracellulaires de HCoV-OC43 hautement purifiées et d'étendre cette approche au SRAS-CoV2. À cette fin, une pureté élevée avec des rendements suffisants est cruciale car les spectromètres de masse détectent les contaminants. Les protéines présentes dans le sérum du milieu de culture cellulaire, ainsi que les protéines portées par les exosomes produits par les cellules ou par les exosomes présentes dans le sérum du milieu de culture cellulaire, sont particulièrement concernées. Nous avons utilisé une série de méthodes pour éliminer les contaminations par les protéines sériques des cultures cellulaires, enrichir les particules virales et séparer les exosomes des virus. Nous avons ainsi obtenu une excellente séparation des virions HCoV-OC43 concentrés des exosomes en utilisant le fractionnement par gradient de densité. Les résultats de spectrométrie de masse sur les fractions purifiées ont validé l'enrichissement en particules virales dans la fraction virale et l'absence de protéines virales dans les échantillons contrôles. Plus intéressant encore, nous avons détecté 69 protéines hôtes uniques à la fraction virale (par rapport aux cellules non-infectées). Ces protéines sont principalement associées à la voie du métabolisme de l'ARN suivie de l'interconversion des métabolites, des enzymes modifiant les protéines et des voies modulatrices de l'activité de liaison aux protéines. Puisque nous avons séparés les exosomes des virus, nous en avons profiter pour évaluer si le virus altère leur contenu protéines. La spectrométrie de masse a de facto identifié 51 protéines uniques aux exosomes produits par les cellules infectées par HCoV-OC43. Celles-ci régulent des voies des protéines

traductionnelles, des enzymes d'interconversion des métabolites et des voies des protéines d'échafaudage. Nos études préliminaires sur l'interférence ARN ont montré que l'inactivation de 14 de ces protéines hôtes modifiait le titre de HCoV-OC43. L'étude des interactions hôte-protéine virale nous permet de mieux comprendre comment les virus tirent parti des cellules hôtes et comment nous pouvons développer de nouvelles thérapies virales.

Mots-clés : HCoV-OC43, Spectrométrie de masse, Interaction hôte-pathogène, Exosomes.

Abstract

Human coronavirus OC43 (HCoV-OC43) is a beta-coronavirus from the *coronaviridae* family. In contrast to SARS-CoV-2, HCoV-OC43 causes upper respiratory tract disease. However, because of their close phylogenic proximity but distinct pathologies, HCoV-OC43 is a very interesting surrogate to study and compare beta coronaviruses. As all viruses, the latter hijack cell machinery proteins to complete their life cycle. Cellular proteins, particularly those incorporated into virions are of particular interest since they often play a vital role in the virus life cycle. Our goal is to employ the proteomic pipeline we developed for HSV-1 to characterize the host proteins associated with highly purified extracellular HCoV-OC43 particles and finally expand it to SARS-CoV-2. To this end, high purity in sufficient yields is crucial as mass spectrometers pick up contaminants. The proteins present in cell culture medium serum, as well as the proteins carried by the exosomes produced by the cells or by the exosomes present in the cell culture media serum, are of particular concern. We utilized a series of methods to eliminate cell culture serum protein contaminations, enrich the viral particles, and separate exosomes from viral particles. For example, we have obtained an efficient separation of concentrated HCoV-OC43 virions from exosomes using density gradient fractionation. Mass spectrometry results on the purified fractions validated the enrichment of viral particles in the virus fraction and the lack of viral proteins in the mock samples. Most interestingly, we detected 69 host proteins unique to the virus fraction (compared to the mock), mostly regulating the RNA metabolism pathway followed by metabolite interconversion, protein modifying enzymes, and protein-binding activity modulator pathways. Since we also purified extracellular exosomes in the process, we probed whether the virus alters their protein content. Mass spectrometry revealed 51 unique proteins exclusively found in exosomes produced by HCoV-OC43 infected cells. These included translational proteins, metabolite interconversion enzymes, and scaffold proteins. Our preliminary RNA interference studies showed that knocking down 14 of these host proteins altered HCoV-OC43 titers. Studying host-virus protein interactions allows us to gain a deeper understanding of how viruses take advantage of host cells, and how we can develop novel viral therapeutics.

Keywords: HCoV-OC43, Mass spectrometry, Host-pathogen interaction, Exosomes.

Table of content

Résumé I

Abstract III

Table of content V

List of Tables VIII

List of Figures IX

Acknowledgments XIII

Chapter 1—Introduction 1

1.1 Human Coronaviruses (HCoVs) 1

1.1.1 Classification 1

1.1.2 Pathology and Impact of HCoVs on Human Health 3

1.1.3 Prevention and Treatments 5

1.1.4 Morphology of Human Coronaviruses 6

1.1.5 Genome structure 7

1.1.6 Structural proteins 9

1.1.6.1 Surface (spike) protein 9

1.1.6.2 Hemagglutinin-Esterase protein 10

1.1.6.4 Membrane protein 11

1.1.6.5 Nucleocapsid protein 11

1.1.7 Non-structural proteins 11

1.1.8 Virus life cycle 12

1.1.8.1 Attachment 14

1.1.8.2 Viral Entry and Uncoating 14

1.1.8.3 Formation of the replication transcription complex (RTC) 14
1.1.8.4 Viral RNA Synthesis 15
1.1.8.5 Assembly and Virion Release 15
1.2 Exosomes 16
1.2.1 Exosome Biogenesis and Biology 16
1.2.2 Exosomes in Viral Infection 19
1.3 Viruses and Methods of Exosome Detection 20
1.3.1 Mass Spectrometry and Viral Proteomics 20
1.4 Hypotheses and Objectives 21
Chapter 2—Materials and Methods 22
2.1 Cell lines 22
2.2 Viral stocks 22
2.3 Virus Concentration Methods 23
2.3.1 Concentrating HCoV-OC43 Using 100 kDa Amicon Filters 23
2.3.2 Concentrating HCoV-OC43 by ultracentrifugation 23
2.4 Virus and Exosome Separation 23
2.5 Western blot and Antibodies 24
2.6 HCoV-OC43 Quantification Using the $TCID_{50}$-IPA Method 25
2.7 Silver Staining 26
2.8 Electron Microscopy 27
2.9 Mass spectrometry 27
2.10 Viability Assay 28
2.11 DsiRNA knock-down 29
2.12 SARS-CoV-2 samples 30

Chapter 3—Results 31
3.1 HRT-18 cells express the CD9 and CD63 Exosome Markers 31
3.2 The Optiprep Density Gradient is an Optimal Method to Concentrate Coronavirions 33
3.3 Efficient Separation of Extracellular Virions from Exosomes 35
3.4 Infectious HCoV-OC43 Particles Overlap with the Viral N Protein Marker Along the Density Gradient 37
3.5 Fractions 6 and 17 Are Strongly Enriched for Intact Exosomes and Virions 38
3.7 Mass spectrometry 42
3.7.1 Fraction 17 from Infected Cells Is Strongly Enriched in Virions 42
3.7.2 The Extracellular Virions and Exosomes Contain Several Unique Proteins 43
3.8 DsiRNA Knock-down 55
3.9 SARS-CoV-2 57
Chapter 4—Discussion 59
4.1 Analysis of Virus and Exosome Fractions 61
4.2 Analysis of MS Results for HCoV-OC43 Virions 61
4.3 Analysis of MS results for HCoV-OC43 infected exosomes 63
4.4 SARS-CoV-2 Virions 64
Chapter 5—Conclusion 65
References 66

List of Tables

Table 1. **Down-regulation of cellular proteins by dsiRNAs** 29

Table 2. **Concentration and total recovery of extracellular virus concentration methods** .. 34

Table 3. **HCoV-OC43 structural proteins enrichment in virus-infected fractions** 43

Table 4. **Unique cellular proteins associated with HCoV-OC43 infected virus fraction** 46

Table 5. **Unique cellular proteins associated with HCoV-OC43 infected exosome fraction** 51

Table 6. **Cellular proteins of interest and their pathways in the virus fraction** 54

Table 7. **Cellular proteins of interest and their pathways in the exosome fraction** 54

List of Figures

Figure 1. ***Coronaviridea*** **family and beta coronavirus subgenus** 2

Figure 2. **Timeline of human coronaviruses** 3

Figure 3. **Comparison of characteristics of β-Coronavirus SARS-CoV-2 and HCoV-OC43** 4

Figure 4. **Structure of Beta-Coronavirus** 6

Figure 5. **Genome organisation of Coronaviruses** 7

Figure 6. **Genome organizations of Coronaviruses** 8

Figure 7. **Organization of the HCoV-OC43 spike (S) protein** 10

Figure 8. **The coronavirus life cycle** 13

Figure 9. **Biogenesis and identification of exosomes** 17

Figure 10. **Structure and composition of exosomes** 18

Figure 11. **ACE2-positive exosomes and SARS-CoV-2 infection** 19

Figure 12. **Schematic overview of extracellular virus concentration and purification** 24

Figure 13. **$TCID_{50}$/ml-IPA using the DAB stain method** 26

Figure 14. **Expression of exosome markers in HRT-18 cells** 32

Figure 15. **Expression of exosome markers in Vero-E6 cells** 33

Figure 16. **Separation of exosomes and virus after fractionation** 36

Figure 17. **$TCID_{50}$/ml-IPA on HCoV-OC43 fractions** 37

Figure 18. **Silver staining of mock and HCoV-OC43- infected fractions** 39

Figure 19. **Inactivation of HCoV-OC43 using paraformaldehyde** 40

Figure 20. **TEM images from exosome and virus fractions** 41

Figure 21. **Cellular protein content of virus and exosome fractions** 44

Figure 22. **Distribution of cellular protein pathways associated with the virus** 45

Figure 23. **Distribution of cellular protein pathways associated with exosome fraction** 50

Figure 24. **Effects of dsiRNAs on reduction of HCoV-OC43 production** 56

Figure 25. **SARS-CoV-2 fractionation** 57

List of abbreviations

ACE2: Angiotensin-converting enzyme 2

β coronavirus: Beta coronavirus

BBB: Blood–brain barrier

CNS: Central Nervous System

CTD: C-terminal domain

DMV: Double-membrane vesicle

DPI: Day post-infection

DsiRNAs: Dicer-Substrate Short Interfering RNAs

E protein: Envelope protein

ER: Endoplasmic reticulum

EV: Extracellular vesicles

FBS: Fetal bovine growth serum

HE protein: Hemagglutinin esterase protein

HSP: Heat-shock protein

HCoV: Human Coronavirus

HCoV-OC43: Human Coronavirus OC43

IBV: Avian infectious bronchitis coronavirus

ILVs: Intraluminal vesicles

M protein: Membrane protein

MERS-CoV: Middle East Respiratory Syndrome Coronavirus

MOI: Multiplicity of infection

MS: Mass spectrometry

N protein: Nucleocapsid protein

NendoU: Nidoviral RNA uridylate-specific endoribonuclease

Nsp : Non-structural proteins

NTD: N-terminal domain

ORF: Open Reading Frame

PFA: Paraformaldehyde

PP1a: Poly protein 1a

RBD: Receptor-binding domain

RTC : Replication-transcription complex

RdRp : RNA-dependent RNA polymerase

SFM Optipro: Serum-free Optipro medium

S protein: Surface (Spike) protein

SARS-CoV-2: severe acute respiratory syndrome coronavirus 2

SsRNA: Single-stranded RNA

$TCID_{50}$/ml-IPA: Median Tissue Culture Infectious Dose- immunoperoxidase assays

TM: Transmembrane domain

VLP: Virus-like particle

WB: Western blot

برای امیر

برای امین

و برای مادرم و پدرم

To Amir

To Amin

And, To my Mom and Dad

Acknowledgments

I would like to thank my supervisor, Dr. Roger Lippé who has supported me during every step of this journey. I am grateful for all the opportunities and guidance you gave me to become a better researcher.

To Amir, thank you for all your love. You believed in me even when I didn't believe in myself. Your presence in my life is a source of strength and joy.

To my mom and dad, your endless love and unconditional support are invaluable to me. No matter the distance, you were always there to listen and provide invaluable guidance when things seemed impossible. To my brother Amin, I can't put into words how much I miss you. Thank you for always having my back and adding fun and laughter to my life!

To Sandrine, thank you for all the delicious cakes you made for us and for the fun plans to get together and lift our moods! It is great to have you in the lab.

To my friends in the lab, Alisa, Bita, Josiane, Christopher, Jonas, and Yulia. Thank you for all your help and support over the past months. We learned a lot together and you all have made my experience here more enjoyable.

To Sara, thank you for being a source of comfort and friendship.

And finally, thanks to all the people at the Université de Montréal that made it possible for me to reach this point of my graduate studies journey.

Chapter 1—Introduction

1.1 Human Coronaviruses (HCoVs)

The story of coronaviruses can be traced back to the 1930s (1) when the avian infectious bronchitis virus (IBV) in newborn chicks was discovered (2). However, it was not until the mid-1960s that scientists found that humans could also be infected with coronaviruses. The first two human coronaviruses found were the human coronavirus OC43 (HCoV-OC43) and 229E (HCoV-229E). These coronaviruses cause mild infections in immunocompetent individuals and so human coronaviruses were not considered highly pathogenic until the outbreak of SARS-CoV (Severe Acute Respiratory Syndrome Coronavirus) in 2002 in the Guangdong province, China (3). As a result of the SARS epidemic, more virus screening and sequencing were conducted, which led to the detection of HCoV-NL63 and HCoV-HKU1 (Hong Kong University) (4). It was ten years after in 2012 that MERS-CoV appeared in the Middle East. In December 2019, an emerging virus called "SARS-CoV-2" with 79.5% sequence identity to SARS-CoV emerged in China and was soon thereafter declared by the World Health Organization (WHO) to be the virus responsible for the COVID-19 pandemic (5). As of June 2023, more than 767 million COVID-19 cases have been declared in over 200 countries, causing more than 6.9 million deaths (COVID-19 Dashboard). SARS-CoV-2 targets upper and lower respiratory tract tissues, and the virus is highly efficient in human-to-human transmission. Symptoms range from asymptomatic infections to acute inflammation and pneumonia, especially in the elderly and those with chronic illnesses (6).

1.1.1 Classification

Coronaviruses belong to the *Nidovirals* order, the *Coronaviridae* family, and the *Orthocoronavirinae* subfamily (7). Coronaviruses are further classified into four genus: α, β, γ, and δ (8). Coronaviruses that are responsible for human infections belong to α and β coronaviruses whereas the γ and δ coronavirus family mostly infect birds (9). Further phylogenetic analysis has subdivided the β coronaviruses into three sub-genuses: subgenus β 2a (*Embecovirus*) with HCoV-

OC43 and HCoV-HKU1 viruses; subgenus β 2b (*Sarbercovirus*) with SARS-CoV and SARS-CoV-2 viruses, and subgenus β 2c (*Merbecovirus*) with MERS-CoV (see Figure 1 for the details) (10, 11).

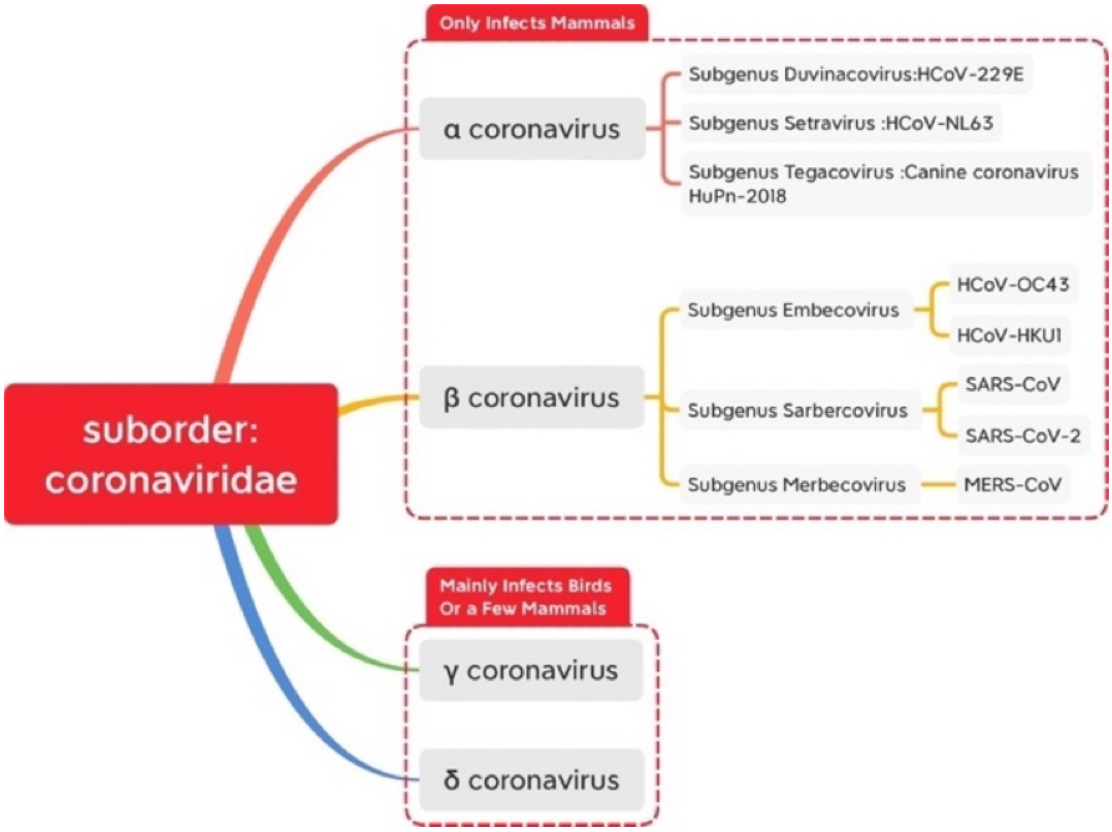

Figure 1. *Coronaviridea* family and beta coronavirus subgenus

The International Committee on Taxonomy of Viruses categorized coronaviruses into 4 genuses: α, β, γ and δ coronavirus. The first two only infect mammals, and the latter two mainly infect birds; Figure from (12).

It is considered that α and β coronaviruses originated from bats, except for HCoV-OC43 and HCoV-HKU1, which originated in rodents (Figure 2). The *α* and β 2a HCoVs, usually cause mild upper respiratory diseases (11, 13), while the highly pathogenic human beta coronaviruses from subgenus *sarbercovirus* and *merbecovirus*, cause severe respiratory syndrome in humans (9).

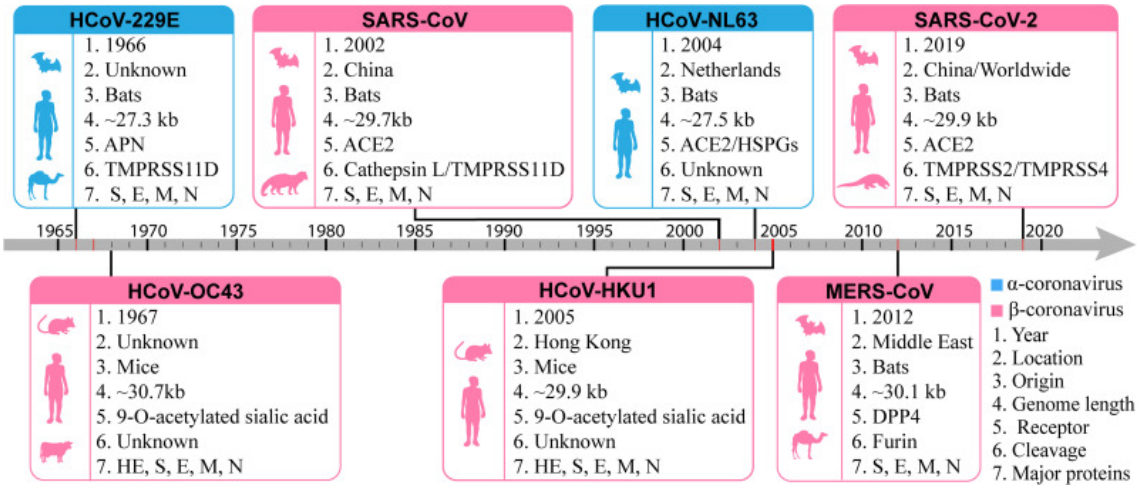

Figure 2. Timeline of human coronaviruses

Summary of when and where each virus was found, the animal of origin, and virus structural proteins S: surface protein, E: envelope protein, M: membrane protein, N: nucleocapsid protein, HE : Hemagglutinin esterase) are shown in each box. The α coronaviruses are shown in blue and, β coronaviruses in pink; Figure from (14).

1.1.2 Pathology and Impact of HCoVs on Human Health

Studies reveal that 4.7% of respiratory infections of viral origin are related to HCoV-OC43 while HCoV-OC43 is the most common coronavirus responsible for upper respiratory infections with mild symptoms. (15, 16). Infection with HCoV-OC43 is subclinical and self-limited, and most of the infections occur in upper respiratory tract cells. According to some reports, patients who have a high risk of developing respiratory tract infections, such as infants, the elderly, or individuals suffering from immunosuppression, have experienced severe HCoV-OC43 infections of the respiratory tract (17). In addition, HCoV-OC43 has been detected in patients with Parkinson's disease and multiple sclerosis (MS), and it has been suggested that the virus may play a role in neurologic disorders (18). There has also been evidence that HCoV-OC43 induces the death of neuronal cells, which is associated with viral persistence and may contribute to a decrease in central nervous system (CNS) functional abilities in animals that survive the infection (19). HCoV-OC43 may also cause gastrointestinal symptoms as well (20). In contrast, SARS-CoV-2 infects the lower respiratory tract and can cause severe respiratory illness, especially in the elderly or those

with chronic illnesses. (21). The comparative characteristics of SARS-CoV-2 and HCoV-OC43 are shown in Figure 3.

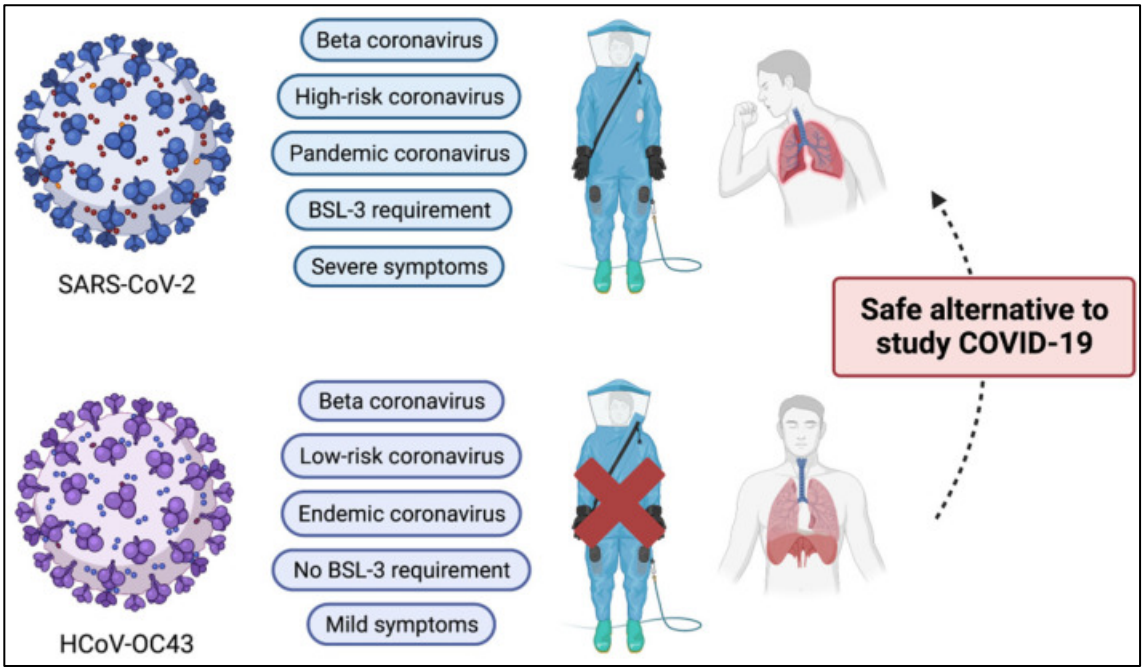

Figure 3. Comparison of characteristics of β-Coronavirus SARS-CoV-2 and HCoV-OC43

HCoV-OC43 can be considered as a surrogate of SARS-CoV-2 as they are both β-*coronaviruses, with the advantage that HCoV-OC43 is a low-risk, endemic coronavirus that only needs biosafety level 2 facilities; Figure from (21).*

SARS-CoV-2 may also exhibit neuroinvasive characteristics and may use a variety of routes to enter the central nervous system (CNS), including the olfactory and trigeminal nerves, cerebrospinal fluid, and the lymphatic system (22). Based on SARS-CoV studies, researchers suggest two pathways to explain how SARS-CoV-2 can enter to the human CNS: the hematogenous entry or the neuronal retrograde dissemination. In the hematogenous entry the virus can enter the brain via the bloodstream, while the in neuronal retrograde dissemination pathway the virus can travel from the peripheral nerves to the brain (23). By the hematogenous route, viral particles spread to the pulmonary blood circulation, then infects the brain microvascular endothelial cells to reach the brain. (24). SARS-CoV-2 may also infect peripheral neurons and enter the CNS by retrograde axonal transport (25). ACE2 is broadly expressed on

the epithelial cells of the oral mucosa, which allows SARS-CoV to reach the brains of hACE2 mice mostly through the olfactory bulb and to spread into the brain via olfactory sensory neuron axons (26). There has also been evidence that SARS-CoV-2 spreads into the CNS through the vagus nerve and the dorsal root ganglia from the lungs, as this pathway is used by other coronaviruses, such as HEV67 (27), and by influenza A (28).

1.1.3 Prevention and Treatments

SARS-CoV-2 inhibitors can affect the virus at different stages of its life cycle, such as entry (spike inhibitors), proteolytic processing (main protease inhibitors, papain-like protease inhibitors), RNA synthesis (NSP12 to NSP16 inhibitors), and assembly (nucleocapsid inhibitors). For instance, Two antiviral drugs which are approved by Health Canada: PAXLOVID (Pfizer) which consists of the anti-protease agent nirmatrelvir and is boosted by the antiretroviral ritonavir (29); and Veklury® (Remdesivir); (Gilead Sciences Canada) inhibits SARS-CoV-2 RNA polymerase (30, 31). Furthermore, several vaccines against SARS-CoV-2 have been approved including viral vector vaccines, such as ChAdOx1-s (AstraZeneca) and AD26.COV2.S (Johnson & Johnson) as well as the mRNA vaccines Spikevax (Moderna) and BNT162b2 (Pfizer/BioNTech)(31). However, as new variants emerge, the efficacy of existing vaccines against infection decreases is questioned (32).

Cellular components, which are involved in virus entry and replication, can also be targeted as therapeutic targets. For instance, coronaviruses use the host cell to hide in double membrane vesicles (DMVs) and replicate there. In this regard, K22 was identified as a small compound targeting membrane-bound coronavirus RNA synthesis by inhibiting DMV formation (33), viral replication, and infectivity in a wide range of coronaviruses such as HCoV-229E, IBV, MERS-CoV, and SARS-CoV (23). Interestingly, exosomes are also being considered for the treatment of viral infections as vaccines and drug delivery vehicles. Exosomes are modified to express receptor-specific ligand molecules on their surface that carry miRNA or siRNA-based therapeutic molecules to specific organs (34, 35). Moreover, ACE2-expressing exosomes (evACE2) are used as therapeutic molecules, competing with cellular ACE2 and neutralizing circulating viruses (36). Extending recent findings regarding small molecules, exosome-based therapies to other human coronaviruses might lead to a pan-corona virus treatment that can be used for both emerging and

remerging human coronaviruses (37). This would provide long-term protection against pathogenic coronaviruses and minimize the need for frequent vaccinations and booster doses Finally, this could reduce the costs associated with the development of new vaccines.

1.1.4 Morphology of Human Coronaviruses

Coronaviruses form enveloped and spherical particles of 70-120 nm in diameter (38). A schematic view of coronaviruses is shown in Figure 4. Coronaviruses possess spike protein (S), which is crucial for their attachment and entry into host cells. The spike protein binds to the receptors of the host, allowing the virus to enter the cell. Beta coronaviruses in the 2A lineage like HCoV-HKU1 and HCoV-OC43 have another surface protein called hemagglutinin-esterase (HE) (9, 39, 40). The coronavirus envelope is comprised of two other proteins: Envelope (E pro) and membrane (M). Inside the envelope, there is a positive single-stranded genomic RNA coated with another structural protein called the nucleocapsid protein (N) (41).

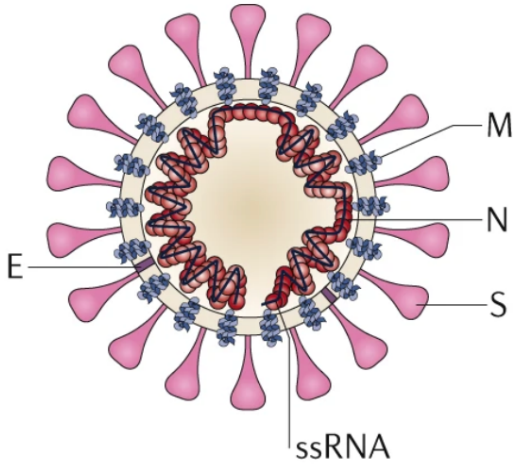

Figure 4. Structure of Beta-Coronavirus

Most of coronaviruses have 4 structural proteins: S, M, E, and N. HCoV-OC43 and HKU1 have another structural protein called HE; Figure from (9).

1.1.5 Genome structure

The genome of coronaviruses is a positive-sense, single-stranded RNA (ssRNA) that is 27-32 kb. The first two-thirds of the viral genome from the 5' end codes for a large open reading frame (ORF). ORF1a and ORF1b are directly translated by cellular ribosomes into two polyproteins: polyprotein 1a and polyprotein 1ab (pp1a and pp1ab) (42). These polyproteins are autoproteolytically cleaved by the viral proteases, generating 16 non-structural proteins that play role in transcription and replication of the virus genome (43). The 3' terminus of the coronavirus genome encodes 4 or 5 structural proteins including the spike (S), envelope (E), membrane (M), nucleocapsid (N), and hemagglutinin esterase (HE). The PP1a, PP1ab, S, E, M, and N proteins are expressed in all *Coronaviridae* family genomes. The mutation rate of coronaviruses is moderate to high when compared to other ssRNA viruses and the S protein gene is the predominant point of these mutations (44). See Figure 5 for more details of HCoVs genome structure.

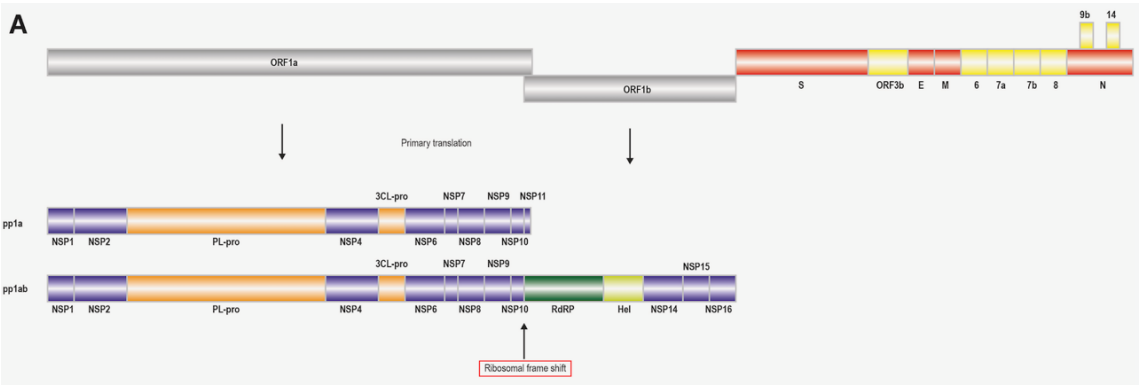

Figure 5. Genome organisation of Coronaviruses

Organization of structural and non-structural proteins of coronaviruses. The frame shift position, which is necessary for the translation of ORF1b and the production of pp1ab is shown in red square. The non-structural proteins are PL-pro: Papain-like protease, 3 CL-pro: Cysteine protease, RdRP: RNA-dependent RNA polymerase and Hel: Helicase. Figure from (45).

Many coronaviruses contain additional ORFs that encode accessory proteins and the role of these proteins in the virus life cycle can be different due to each specific coronavirus (Figure 6). For example, in the HCoV-OC43; the 3' terminus codes for accessory proteins 5a and 7b (46). It is suggested that the 5a has cyclic phosphodiesterase activity, which may modulate cAMP-mediated signaling and vital physiological processes such as lipid metabolism and apoptosis (47).

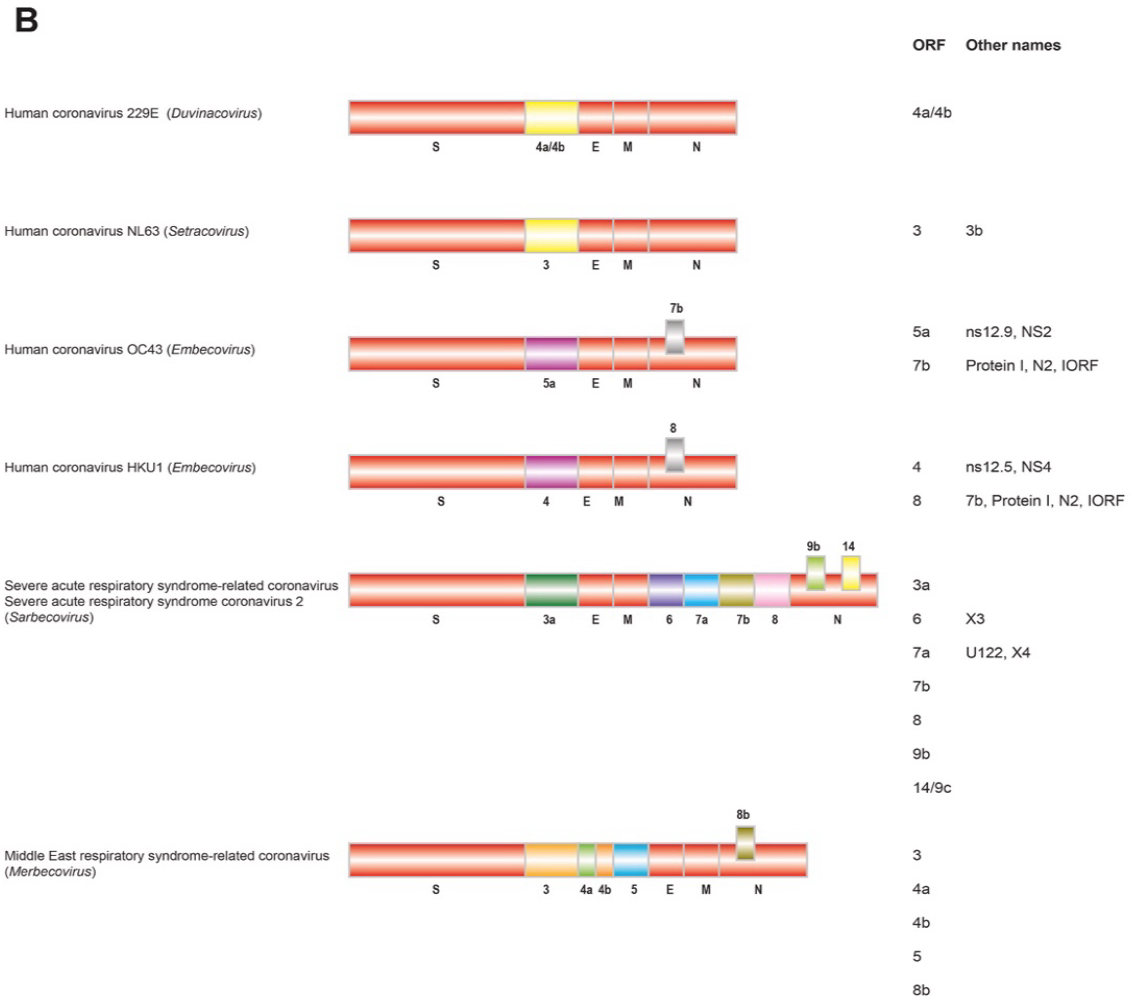

Figure 6. Genome organizations of Coronaviruses

Organization of accessory proteins of alpha and beta coronaviruses. HCoV-OC43 possesses 2 ORFs for the expression of accessory proteins; Figure from (45).

The SARS-CoV-2 genome also codes for eight accessory proteins such as ORF3a, ORF3b, p6, ORF7a, ORF7b, ORF8b, ORF9b, and ORF14 (48). These accessory proteins regulate viral replication and modulate the host immune response although the exact role of these accessory proteins needs more investigation (9, 49-51).

1.1.6 Structural proteins

1.1.6.1 Surface (spike) protein

The S protein is a type I transmembrane protein with a molecular weight of 128-160 kDa before glycosylation and 150-200 kDa after N-linked glycosylation (39). The *Coronaviridae* family spike protein is a multifunctional protein that plays a critical role in mediating the attachment, fusion and entry of the virus into host cells (39, 52). The S protein is composed of two subunits, S1 and S2. The S1 subunit is responsible for receptor binding and recognition, while the S2 subunit orchestrates the subsequent fusion of viral and host membranes (45). In HCoV-OC43, the S protein is involved in receptor binding and hemagglutination (16). The S1 subunit Contains two distinct domains, the N-terminal domain (NTD) and the C-terminal domain (CTD). In HCoV-OC43 the NTD of S1 is responsible for sugar receptor binding .The CTD has a receptor binding domain (RBD) that interacts with cellular proteins in other coronaviruses , see Figure 7 (52, 53).

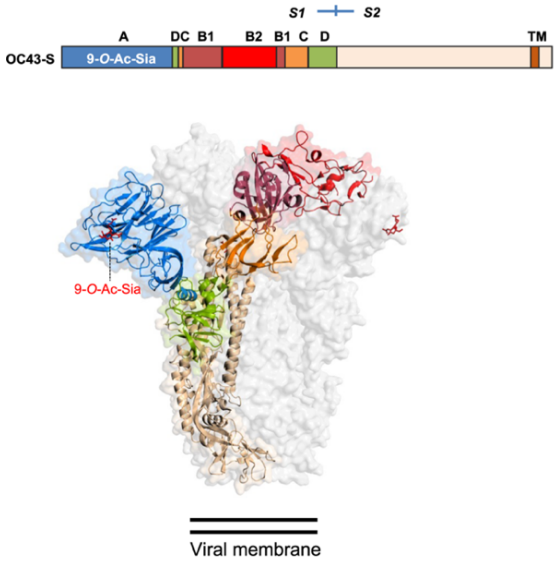

Figure 7. Organization of the HCoV-OC43 spike (S) protein

Upper part: The HCoV-OC43 S protein subunits (S1 and S2) are shown above. The S1 domain contains 9-O-acetylated sialic acid (9-O-Ac-Sia) receptor binding and the S2 contains the transmembrane domain (TM). Lower part: cryo-EM structure of the trimeric HCoV-OC43 S; Figure from (54).

1.1.6.2 Hemagglutinin-Esterase protein

The HE protein is a 40-50 kDa type I transmembrane protein, which is only present on the surface of the beta coronaviruses 2a: HCoV-OC43 and HCoV-HKU1. HE protein has a carbohydrate-binding ("lectin") domain and a acetyl esterase domain (55). It has been reported that through evolution and the adoption of HCOV-OC43 into human upper respiratory sialo-glycoproteins, a combination of mutations has occurred in the HE lectin domain, resulting in impaired HE receptor binding ability (55, 56). Due to that it is suggested that successful virus attachment requires a balance between the S protein attachment and HE esterase activity to destroy the decoy receptors and attach to functional cell receptors. Moreover, HE esterase activity plays an important role in the release of infectious particles from host cells (56). It has been shown that HCoV-OC43 lacking HE protein, or with a HE protein lacking functional acetyl-esterase enzymatic activity, was unable to produce infectious viral particles (39, 40).

1.1.6.3 Envelope Protein

The E protein is a small 8-12 kDa integral membrane protein. While the virus utilizes protein expression machinery to produce high levels of E protein, only small amounts of the protein are found in the virion envelope (57). Current evidence suggests oligomerization of the E protein results in the formation of ion channels. In SARS-CoV and IBV, ion channel activity affects virion release and contributes to viral pathogenesis (39). Studies on the HCoV-OC43 E protein revealed it is required for the production of infectious viruses. Furthermore, the E protein is responsible for the development of neurovirulence in animals (58).

1.1.6.4 Membrane protein

The M protein is a 25-30 kDa transmembrane protein and the most abundant structural protein in the virus envelope. The M protein is and interacting with other viral structural proteins during the assembly of the coronavirus particle (39, 59). Moreover, the M protein is essential for virion morphogenesis. S, M and E proteins interactions form the viral envelope which is sufficient for the production of virus-like particles (60).

1.1.6.5 Nucleocapsid protein

The N protein is a 45-50 kDa RNA-binding protein, which binds to newly synthesized RNA to form a helically symmetric nucleocapsid that is critical for viral genome packaging. The N protein is involved in RNA packaging, viral genome replication, and evasion of immune responses (61, 62). For example, the N protein of SARS-CoV-2 acts as a viral inhibitor of RNAi in host cells (63). Studies suggested that the SARS-CoV-2 N protein with viral RNA and other viral proteins, like nsp-12, are involved in liquid-liquid phase separation (64, 65).

1.1.7 Non-structural proteins

The coronavirus genome codes for 16 non-structural proteins (Nsp): Nsp1-Nsp16. Nsp1 is the most N-terminal cleavage product of the polyproteins and is a leader protein. It is a host translation inhibitor that degrades host mRNAs by binding to 40 S ribosomes and inactivates their translational functions (66). Nsp2's exact functions and structure remain unclear but it has been

reported that Nsp2 has a highly conserved cysteine residue which may serve for an RNA-binding role (67). Nsp3 is a papain-like proteinase (PLpro) and Nsp5, a 3 C-like proteinase (3CLpro), are the two viral proteases that cleave pp1a and pp1ab into 11 and 16 smaller subunits, respectively (68). Nsp4 involves in the formation of viral replication transcription complex (RTC) and it helps modify ER membranes with Nsp6 (69). Nsp7 is an RNA-dependent RNA polymerase (RdRp) that forms a complex with 2 other RdRps: NSP8 and NSP12 to yield the RNA polymerase activity of NSP8 (70). Nsp 9 is an RNA-binding protein that interacts with RdRp/Nsp12 to form RTC (71). Nsp10 is a cofactor for Nsp16 and Nsp14, which mediate the proofreading exonuclease activity (72). Nsp 11's exact role has not been characterized yet. Nsp13 contains an N-terminal zinc-binding and C-terminal helicase domain which exhibits a variety of enzymatic activities including NTPase, dNTPase, and RNA/DNA helicase activity (73). Nsp14 is a highly conserved Nsp known for its 3’ to 5 ’ proofreading Exoribonuclease activity, mediating RNA capping together with Nsp10, Nsp12, Nsp13, and Nsp16 (74). Nsp15 is a nidoviral RNA uridylate-specific endoribonuclease (NendoU) that participates in viral replication and is a type I interferon antagonist (39). Finally, Nsp16 is a methyltransferase enzyme that is only active in the presence of its activating partner Nsp10 and exhibits RNA cap (nucleoside-2’-O)-methyltransferase activity (75).

1.1.8 Virus life cycle

The HCoVs replication cycle starts from attachment of virus to permissive host cells, followed by entry and uncoating, expression of the viral non-structural protein and enzymes, synthesis of viral RNAs and finally assembly and egress of newly synthesized viruses. A schematic picture of the virus life cycle is shown in Figure 8.

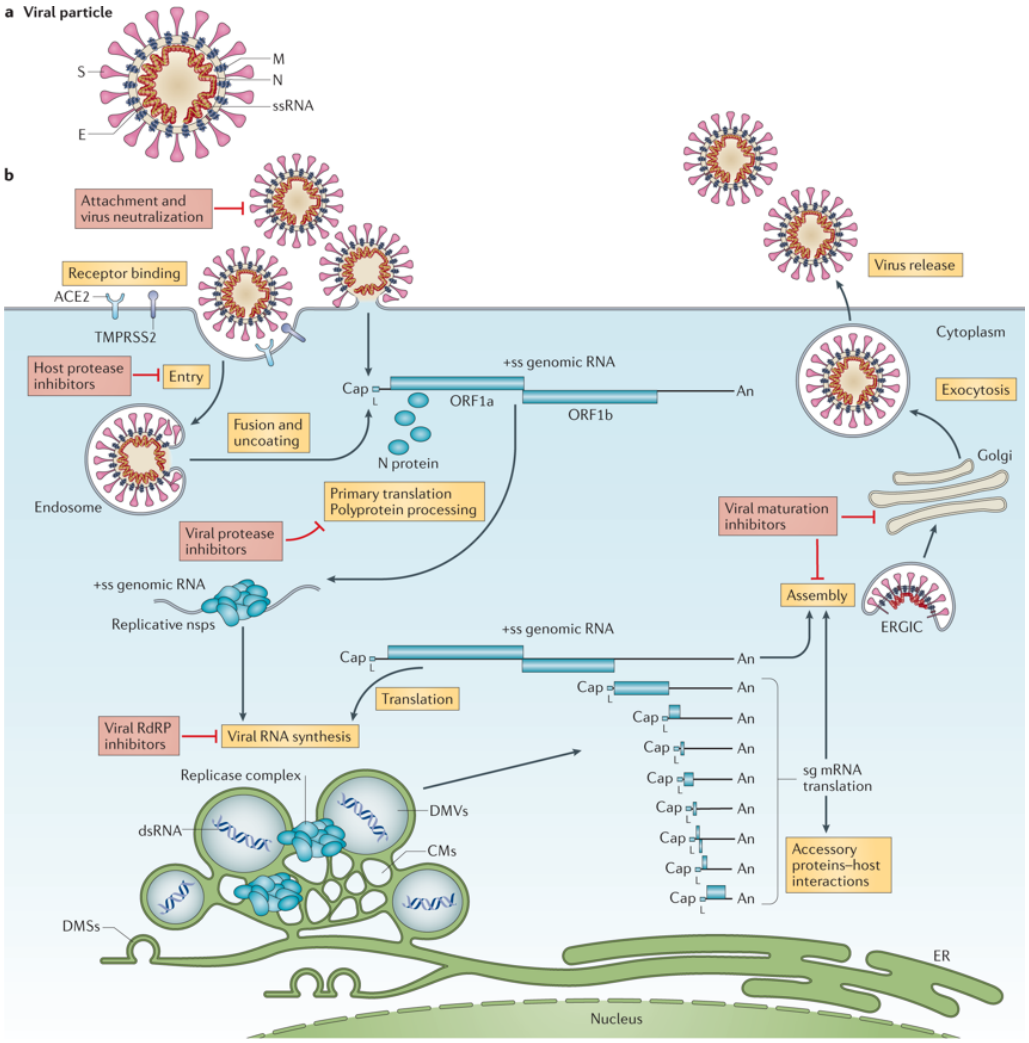

Figure 8. The coronavirus life cycle

The HCoVs life cycle starts with the attachment of the virus S protein to the cellular surface receptors. Following, the virus S protein undergoes conformational changes that allow it to enter the target cell. The virus genome is translated into the main polyproteins (PP1a and P1Pab) and non-structural proteins are produced. Non-structural proteins make a replication-transcription complex which is responsible for the synthesis of genomic RNA as well as the transcription of sub genomic mRNA in DMV compartments. The newly synthesised virus RNA moves to the ERGIC, interacts with pre-synthesised structural proteins, and the complete virion exits from the cell by

exocytosis. Abbreviations: cap, 5' cap structure; dsRNA, double-stranded RNA*; L, leader sequence; RdRp, RNA-dependent RNA polymerase, Figure from (46).*

1.1.8.1 Attachment

Coronaviruses attach to cells using the RBD site in the S1 subunit of the S protein. That domain specifically binds to the host cell receptor, which is angiotensin-converting enzyme 2 (ACE2) for SARS-CoV-2 and SARS-CoV, dipeptyl peptidase4 for MERS-CoV (76) and, 9-O-acetylated sialic acid or HLA class I molecules for HCoV-OC43 (77, 78). Most of the α-coronaviruses use aminopeptidase N (CD13) for cell entry while HCoV-229E binds to aminopeptidase N (APN) (79).

1.1.8.2 Viral Entry and Uncoating

During entry, the S2 domain undergoes conformational changes with the assistance of cellular proteases. The fusion step happens through one of two pathways on endocytosis membranes or at the cell surface (78). It is suggested that HCoV-OC43 is trafficked to endosomes through a caveolin-mediated and dynamin-dependent route (78) while SARS-CoV-2 directly fuses with the plasma membrane using S2 conformational changes induced by host proteases such as TMPRSS2 or go through the low pH endosomal pathways (80).

1.1.8.3 Formation of the replication transcription complex (RTC)

The coronavirus genome is released into cytoplasm and the genomic-positive ssRNA serves as a transcript for the translation of ORF1a into pp1a. Expression of ORF1b requires a ribosomal frameshift which leads to the translation of ORF1b and the production of pp1ab (47). As a result of proteolytic cleavage by the viral proteases, the non-structural proteins that are responsible for virus replication and transcription form the replication transcription complex (RTC) are produced (46, 81). Other nsps, including nsps 3, 4, and 6, rearrange the membrane of the ER to form organelle-like structures called double-membrane vesicles (DMVs) where coronaviruses organize their genome transcription to evade the host immune system (47, 82). In DMVs, the virus RdRP makes sub-genomic mRNAs that encode structural and accessory proteins as well as a full-length ssRNA negative sense that acts as a template for viral RNA synthesis (5).

1.1.8.4 Viral RNA Synthesis

In the RTC compartments, genomic RNA is used as a template for the synthesis of intermediate negative sense RNAs, which then become templates for new copies of the viral genome. During the synthesis of negative-sense RNA, the polymerase enzyme switches templates at short motifs called transcription-regulated sequences (TRS) (83). This results in the production of a 5'-nested set of negative sense sgRNA that encodes structural and accessory proteins (84). It is important to note that replication and transcription can also be affected by factors other than RTC, such as viral structural proteins and host proteins. As an example, the Coronavirus structural N protein plays a role in template switching during sgRNA synthesis. Host proteins including heterogeneous nuclear ribonucleoprotein A1, mitochondrial aconitase, polyadenylate-binding protein and polypyrimidine tract-binding protein, may be involved in Coronavirus RNA synthesis through their association with RNA (39, 46).

1.1.8.5 Assembly and Virion Release

Following replication and sub-genomic RNA synthesis, the translation of S, M, E, and HE proteins start in the ER. These proteins move into the endoplasmic reticulum-Golgi intermediate compartment (ERGIC) to join the viral genomes that are encapsidated by the N protein (85). Membrane assembly is initiated by the M protein, which interacts with other structural proteins like S and E to provide the scaffold for virion. Assembly of the virion is completed by the interaction of nucleocapsids and envelope components. After assembly, progeny virions are trafficked to the plasma membrane via the secretory pathway and released by exocytosis (85, 86). The host cytoskeletal also participates in HCoVs assembly and release. For instance, the interaction between tubulin and the cytosolic domain of the S protein is required for the assembly and release of infectious virions (39).

1.2 Exosomes

1.2.1 Exosome Biogenesis and Biology

Exosomes originate from intracellular membranes and mediate cell-to-cell communications. Exosome contents vary depending on which host cell they originate from. Exosomes can carry proteins, lipids, and nucleic acids from both cell and infectious particles like viruses during the process of being released into the extracellular milieu (87). It is believed that cells secrete membrane vesicles which are derived from the endosomes or plasma membranes into the extracellular space called Extracellular vesicles (EVs). EVs are membrane-bound bilayer phospholipid membrane structures and can be categorized into two groups depending on their origin and size: Ectosomes and Exosomes. Ectosomes are EVs formed by direct budding of the plasma membrane, referred to as microvesicles, and large vesicles which are different in size vary from 50 nm to 1 μm (88).

Exosomes originate from late-stage endosomes and are smaller than ectosomes; the exosomes size ranges from 40 to 160 nm (89, 90). Exosomes are released by cells upon the fusion of one of the intermediate compartments of the endocytic system with the cell membrane (91). During the maturation of early endosomes, endosomal membranes are invaginated by ESCRT-dependent or ESCRT-independent mechanisms which result in the production of ILVs (92). Following this, the ILVs are grouped together into a multivesicular body (MVB), which is then able to fuse with lysozymes and undergo degradation or to fuse with plasma membranes and release exosomes into the extracellular space (93, 94). The tetraspanin proteins CD9, CD63, and CD81 are highly enriched in exosomes and can be used for their identification. (95). The pathways involved in the biogenesis of exosomes in cells are shown in Figure 9.

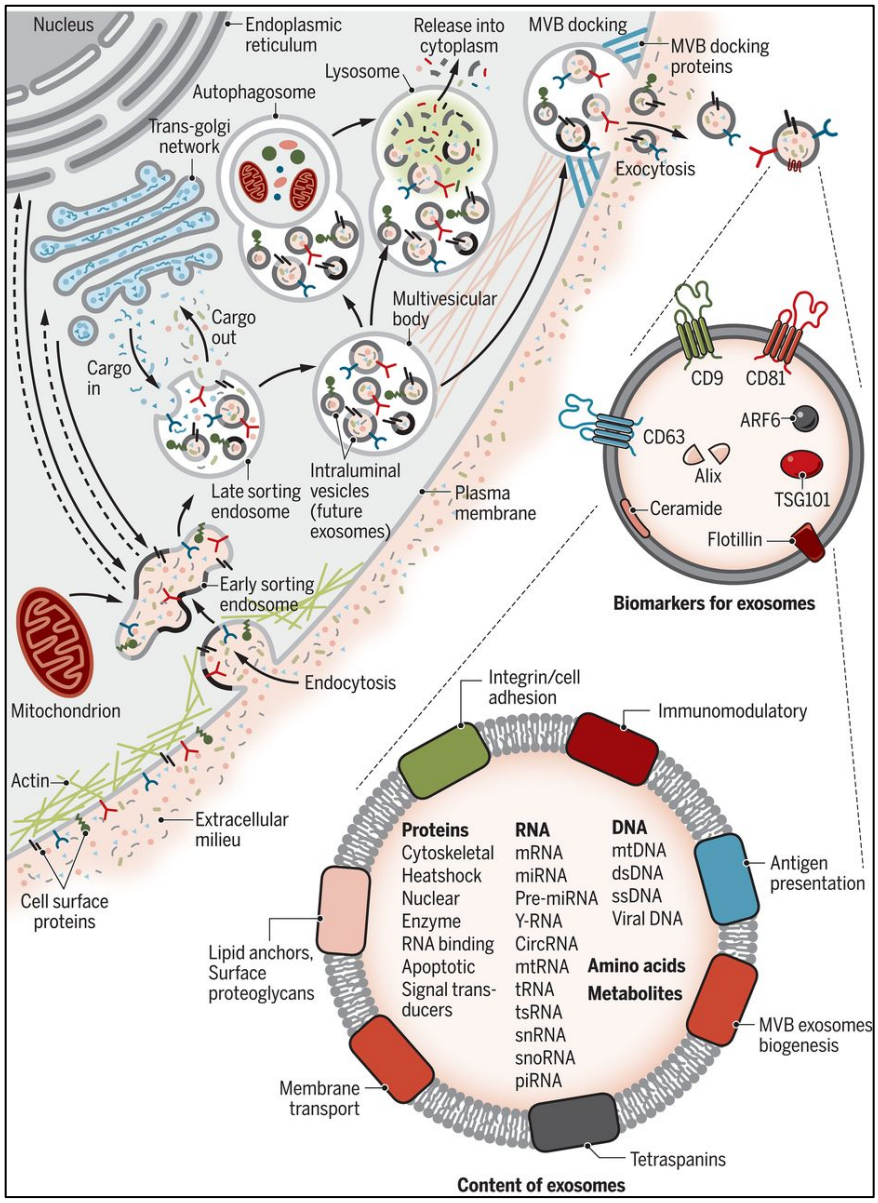

Figure 9. Biogenesis and identification of exosomes

Exocytosis of MVBs results in the release of exosomes with a lipid bilayer composition similar to the plasma membrane. Several proteins are used as markers for exosomes (CD9, CD81, CD63). The exosomes can contain a wide variety of proteins, including cell surface proteins, intracellular proteins, RNA, DNA, amino acids, and metabolites. Figure from (96).

Exosomes contain proteins, DNA, mRNA, microRNA, cellular metabolites and heat-shock proteins (HSP) from cells or infectious particles (97) (Figure 10). Most HSPs are molecular chaperones responsible for protecting the proteome from environmental stresses such as viral infections and reactive oxygen chemicals. It is suggested that the HSPs activate the immune system cells, and different types of HSP compositions in the exosomes activate specific immune cells such as macrophages or NKT cells in response to environmental stress (98). Exosomes have a vital role in cell-to-cell communication and play a significant role in cancer progression, immune system alterations, cardiovascular and central nervous system diseases, and viral infection and pathogenesis (96). Exosomes with different content can cause different responses in target cells, so scientists are using this to produce engineered exosomes as therapeutic agents. As an example, exosomes may contain chemotherapeutic drugs or interfering RNAs that can be directed to specific target cells to be used in the treatment of certain diseases (96, 99).

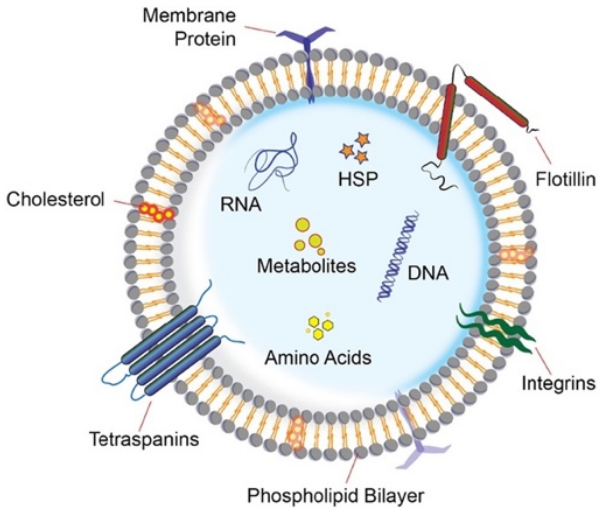

Figure 10. Structure and composition of exosomes

Exosome contains cellular and infectious particles proteins, DNAs ,RNAs and heat-shock proteins(HSP). Exosomes exhibit antigen markers on their surface that can be targeted for their detection like tetraspanin proteins; Figure from (100).

1.2.2 Exosomes in Viral Infection

Viruses can take advantage of exosomes to carry their genome or proteins. For example, Hepatitis B and C viruses can be transmitted from cell to cell via exosomes to evade detection by the host immune system (101). In contrast, some studies have shown that ACE2-expressing extracellular vesicles (evACE2) present in the plasma of patients with COVID-19 neutralize SARS-CoV-2 by competitive binding to ACE2 (Figure 11) (102). Indeed, there was an association between higher levels of ACE2-positive exosomes and milder symptoms and a shorter recovery period (103) (Figure 11). In addition, reduced mortality from SARS-CoV-2 infection was seen in hACE2 mice with an increase of ACE2-positive exosomes (104), suggesting new treatment strategy for COVID-19. Moreover, mass spectrometry (MS) studies on the composition of exosomes from patient's plasma samples during SARS-COV2 infection show that in patient with severe disease, the exosome proteome is associated with chronic inflammation (102).

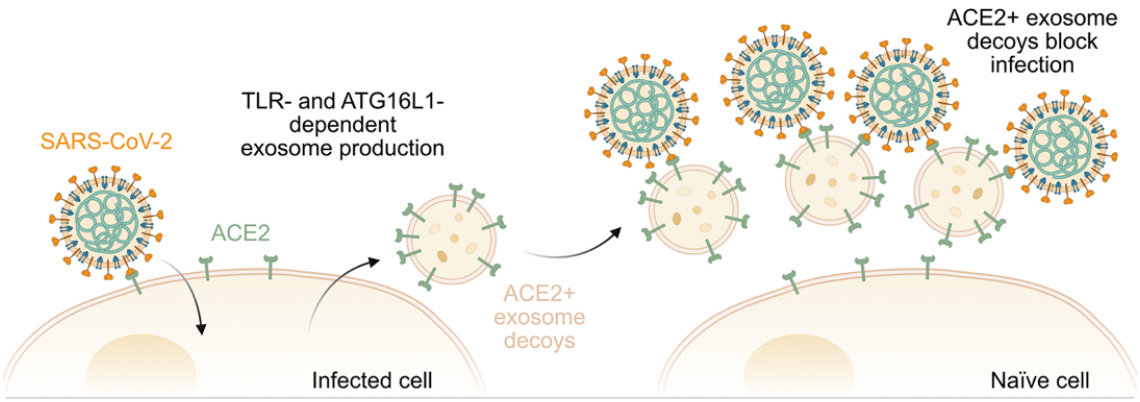

Figure 11. ACE2-positive exosomes and SARS-CoV-2 infection

Exosomes expressing ACE2 mimic endogenous receptors which limit SARS-CoV-2 infection and disease severity, Figure from (103).

1.3 Viruses and Methods of Exosome Detection

1.3.1 Mass Spectrometry and Viral Proteomics

Viruses hijack host by interacting with intracellular proteins, facilitating viral replication, and evading immune defenses. Studying viral-host protein interactions is important to understand the mechanisms of viral infection and the host response as well as develop new strategies to treat and prevent diseases. Proteomics is a high-throughput technology to assess protein-protein interactions by mass spectrometry (MS) (105). In previous studies, SARS-CoV virions subjected to proteomic analysis confirmed the presence of S, M, and N proteins. This method failed to detect the E protein, a single E peptide was detectable by SDS-PAGE followed by electrospray ionization-MS/MS, suggesting that it may be present in low abundance (106).

Analyzing samples using mass spectrometry detects contaminants as well. These can come from a variety of sources, including cell constituents, during sample preparation and cell culture media. (107). MS sample preparation, especially of viral samples can be a double-edged sword, as increasing sample purity and reducing contaminants can result in loss of low abundance proteins. To determine the most accurate results, it is necessary to choose the right negative and positive controls (106, 107). Of particular concern is the presence of exosomes in the preparations of mature extracellular virions as they are released from cells, are abundant in serum and exhibit similar properties as viruses (size, density and even some content). It is thus critical to efficiently separate virions from exosomes.

1.4 Hypotheses and Objectives

Since viruses take advantage of cells to complete their viral life cycles, the investigation of host-pathogen interactions is critical. We hypothesize that the cellular proteins that are incorporated in purified extracellular viral coronavirus particles modulate the viral life cycle. We have already validated this in the context of herpes simplex virus type 1 (108). We further hypothesize that the coronavirus infection alters the composition of exosomes, either for the virus benefit or as an anti-viral strategy by the infected cells. Our goal is 1) Establish a protocol to obtain highly enriched extracellular virions 2) Separate and purify HCoV-OC43 from extracellular vesicles using density gradient-ultracentrifugation 3) Identify the host protein content of extracellular HCoV-OC43 by mass spectrometry 4) Determine the impact of knockdown of host proteins on HCoV-OC43 titer, and 5) Apply our proteomics pipeline to the SARS-CoV samples. Note that all the work with SARS-CoV-2 is done in collaboration with Dr. Nathalie Grandvaux, whose lab provided us with unpurified and inactivated SARS-CoV-2 extracellular samples.

We initially selected HCoV-OC43 as our representative beta-coronavirus because it shares similarities with other beta-coronaviruses such as SARS-CoV-2 and can be manipulated in a biosafety level 2 laboratory. Furthermore, studying HCoV-OC43's interactions may provide valuable insight into the broader family of beta-coronaviruses. Ultimately, it is hoped that comparing the two coronaviral proteomes will ultimately provide valuable clues as to the higher virulence of SARS-CoV-2. In the present work, we therefore designed a purification protocol to enrich extracellular coronaviruses that are depleted of exosomes (both from serum and produced by cells) and then determine their host and viral content by MS. We also took advantage of the distinct purification of exosomes to submit them to a proteomic analysis. Those findings are here presented for HCoV-OC43, and 19 of these host proteins were knocked-down with dsiRNAs. Additional preliminary SARS-CoV-2 results have been obtained, and more samples are ready to be sent for MS analysis. This work will allow us to compare the host protein content of the two beta coronaviruses, see how infection impacts exosome content, and elucidate how these proteins might influence the beta coronavirus life cycle and impact viral propagation.

Chapter 2—Materials and Methods

2.1 Cell lines

The human adenocarcinoma HRT-18^{-} cell line was used for HCoV-OC43 infection and virus quantification (Gift from Dr. Talbot, INRS). Media used for this cell line was Dulbecco modified Eagle medium (DMEM) with 10% fetal bovine growth serum (FBS), 1% L-glutamine (G7513; Sigma-Aldrich), and 1% penicillin/streptomycin (P4333; Sigma-Aldrich). Vero-E6 (ATCC CRL-1586) grown with DMEM with 5% bovine growth serum (BGS), 1% L-glutamine (G7513; Sigma-Aldrich), and 1% penicillin/streptomycin (P4333; Sigma-Aldrich) was used to check the exosome markers for later SARS-CoV-2 experiments. The OptiPRO™ SFM (12309019; Gibco) media is used for HCoV-OC43 production to reduce extracellular contaminants like bovine serum for more accurate MS results. The cell line was checked regularly for mycoplasma contamination.

2.2 Viral stocks

HCoV-OC43 variant VR-1558 (ATCC, Manassas, VA, USA) was used for infection. HRT-18 cells were grown on three Corning™ 245 mm square dishes until 80% confluence. Cells were mock treated or infected with HCoV-OC43 virus at a multiplicity of infection (MOI) of 0.1. Plates were incubated at 37°C, 5% CO_2 on a shaker for 1 h and 12 mL of infection media (Roswell Park Memorial Institute medium (RPMI) (Wisent) with 0.1% of bovine serum albumin (BSA) (Sigma-Aldrich). After 1h, cells were washed once with 1X Phosphate-buffered saline (PBS) then 70 ml of OptiPRO media, and 1% Penicillin-Streptomycin were added to each plate and incubated at 33°C, 5% CO_2 for 3 days. The viruses released into the supernatant were then harvested and concentrated.

2.3 Virus Concentration Methods

2.3.1 Concentrating HCoV-OC43 Using 100 kDa Amicon Filters

At 72 hours post-infection, the supernatant from the above 3 large dishes of infected cells was collected and centrifuged at 1,200 rpm for 5 mins followed by filtration with a 0.45 µm filter. In the next step, the supernatant was concentrated using a single Amicon® Ultra-15 Centrifugal Filter Unit with a 100-kDa cut-off (UFC9100; Millipore). The concentrated extracellular virions were finally diluted in 1.5 ml of 1X PBS and kept at -80°C.

2.3.2 Concentrating HCoV-OC43 by ultracentrifugation

As a second option, the supernatant from the above large plates was collected and centrifuged at 800 g for 10 min at 4° C to pellet cell debris and the supernatant filtered with a 0.45 µm filter. The filtrated supernatant was then put into 12 ml SETON-thin wall-open-top polyclear centrifuge tubes (Seton scientific; NC9863486) and ultracentrifuged in a Hitachi ultracentrifuge (CP-100NX) P40ST rotor at either of 3 different speeds (20, 60 or 100 x 10^3 *g*) at 4° to pellet down the virus and compare yield and enrichment levels at different speeds. After ultracentrifugation, the supernatant was discarded, and the pellet diluted in 200 µl of 1X PBS overnight at 4°C.

2.4 Virus and Exosome Separation

The separation protocol using iodixanol/sucrose gradient was obtained from Dogrammatzis C et al, which successfully reported the separation of HSV-1 viral particles from exosomes (109). The Optiprep/sucrose density gradient was prepared by diluting Optiprep 8% and 25% (Sigma; D1556; contains 60% iodixanol) with 10 mM Tris (pH 8) and 0.25 M sucrose. The biocomop gradient station was used to make continuous gradients from 8 to 25% (with 1% increments in Optiprep concentration) for a total of 18 fractions. Since Amicon concentration proved more efficient than ultracentrifugation (see results below), 1 ml of concentrated virions using the former approach was loaded on top of the continuous gradient .The samples were then ultracentrifuged in a Hitachi (CP-100NX) in a P40ST rotor at 250,000 G for 135 min. Eighteen 600 µl fractions were

manually collected from the top to the bottom of the gradient. A schematic overview of the concentration and separation steps is summarized in Figure 12.

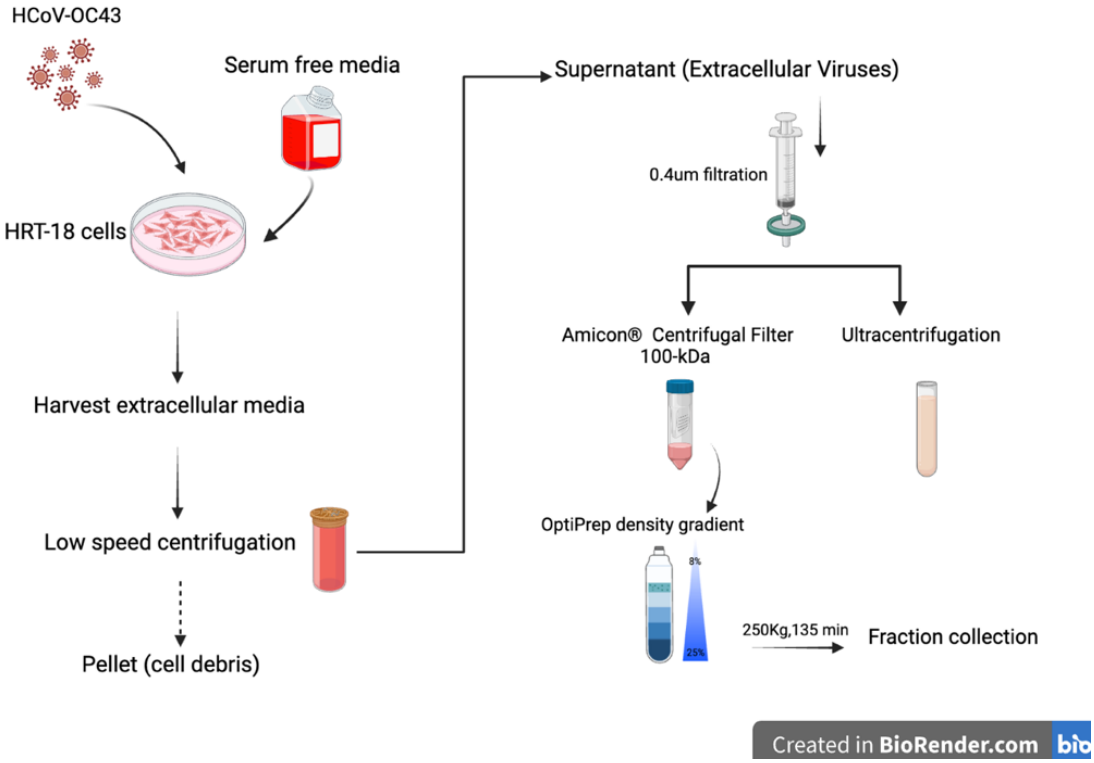

Figure 12. Schematic overview of extracellular virus concentration and purification

Figure created using Biorendre.com.

2.5 Western blot and Antibodies

Equal volumes (50 µl) from each Optiprep fraction were mixed with loading buffer (final concentration: 50 mM Tris-HCl, pH 6.8, 2% SDS, 0.1% bromophenol blue, 10% glycerol, and 2% β-mercaptoethanol) and heated at 95°C for 5 minutes. Samples were then loaded and run on 5 to 20% SDS-PAGE gradient gels and transferred to a PVDF membrane (#1,620,177; Bio-Rad). Membranes were blocked for 30 minutes in 5% skimmed milk in PBS-Tween (13.7 mM NaCl, 0.27 mM KCl, 0.2 mM KH2PO4, 1 mM Na2HPO4, 0.1% Tween 20). Primary antibodies diluted in 5% BSA (A7906; Sigma-Aldrich) in PBS-Tween were added to the blots, incubated overnight at 4°C, washed three times using PBS-Tween, followed by 1h incubation at RT in 5% skim milk in PBS-Tween containing relevant secondary antibodies. Finally, membranes were washed, and the

proteins are revealed with ECL substrate (170-5060; Bio-Rad) using a Chemidoc (Bio-Rad). Primary antibodies used for Western blotting (WB) were from the following sources and dilutions: Rabbit monoclonal anti-CD9 (1:1000; cell signaling, #13,174), Rabbit monoclonal anti-CD63 (1:1000, Abcam -134045), Mouse monoclonal Antibody CD81 (1:500, Santa Cruz; sc-23962), Monoclonal anti-HCoV-OC43 Nucleocapsid protein (1:1000, Millipore Sigma, MAB9012), Rabbit polyclonal anti-SARS-CoV-2 S protein (1:1000; Invitrogen, PA1-41165). Secondary antibodies were purchased from molecular probes and Jackson Immuno-Research.

2.6 HCoV-OC43 Quantification Using the $TCID_{50}$-IPA Method

It was previously demonstrated in our lab by Christopher Savoie (110) that the $TCID_{50}$/ml (median tissue culture infectious dose) assay is more sensitive and reliable than plaque assays for HCoV-OC43 titration. Aside from that, the $TCID_{50}$-IPA (median tissue culture infectious dose by immunoperoxidase staining) method stands out as the most sensitive among different $TCID_{50}$/ml quantification methods ($TCID_{50}$-CPE, $TCID_{50}$-IFA, and $TCID_{50}$-IPA) and is simpler, quicker, and cheaper.

Three days before infection HRT-18 cells were seeded in 96-well plates at 70,000 cells/ml, in DMEM with 10 % FBS at 37°C with 5% CO_2. On the infection day, the media was removed, cells were infected with 50 µL of a serial 10-fold dilution of virus (3 replicates), and incubated at 37°C, 5% CO_2 on a shaker for 1 h for viral adsorption. After 1h, 50 µL of infection media (DMEM 2% FBS, 1X L-Glu, 1X P/S) was added and plates were incubated at 33 °C, 5% CO_2 for 3 days. Three days post-infection (DPI) the media was removed, cells were washed with1X PBS , fixed with 100% methanol containing 0.3% (v/v) hydrogen peroxide for 15–30 minutes at room temperature. Fixative was removed, plates were air-dried, and incubated with HCoV-OC43 S protein Hybridoma primary antibody (dilution1:50) (Gift from Dr. Talbot, INRS, QC, Canada) for 2 h at 37°C with 5% CO_2. Plates were washed three times with 1X PBS and incubated with secondary goat anti-mouse IgG (H+L) (Jackson Laboratory, Bar Harbor, ME, USA) (1:2000 dilution) for 2 h at 37°C <u>without CO_2</u>. Finally, plates were washed 3 times with 1X PBS , 30–40 mg/100 ml of 3.3 'Diaminobenzidine (DAB) containing 0.01% (v/v) H_2O_2 was added, incubated for 15 mins at RT, and the wells were

scored as positive or negative using an Evos XL Core microscope with a 20X objective (Invitrogen, Waltham, MA, USA). Figure 13 graphically details this protocol.

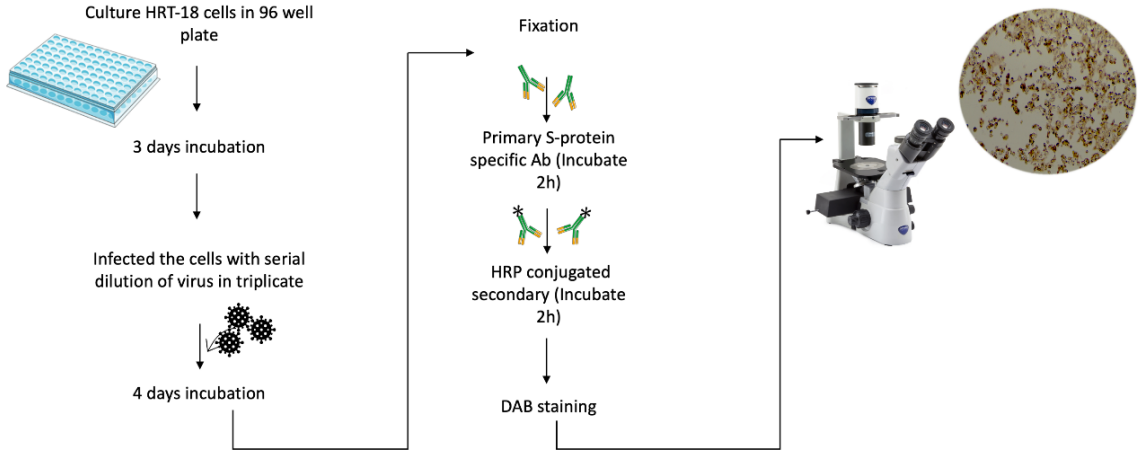

Figure 13. $TCID_{50}$/ml-IPA using the DAB stain method

The median tissue culture infectious dose ($TCID_{50}$/ml) is defined as the dilution of the virus necessary to infect 50% of cell cultures. It was calculated according to the Spearman & Karber method (111) with the following formula: $TCID_{50}$/ml = log (highest dilution giving 100% positive wells) + 0.5 – (total number of positive wells/number of wells per dilution). Figure created using Biorendre.com.

2.7 Silver Staining

Equal volumes (50 µl) of mock and infected exosome and virus fractions were loaded on 5 to 20% SDS-PAGE gradient gels. At the end of electrophoresis, the gels were incubated with fixative buffer (10% acetic acid; 40% methanol in demineralized water) on a shaker for 1 hour. The gels were washed in demineralized water for 10 minutes, 5 times. In the next step, the gels were activated by adding the staining activator (0.02% sodium thiosulphate in demineralized water) for 1-2 minutes. The stain activator was discarded and quickly rinsed twice with demineralized water. The silver solution (0.1 g silver nitrate, 40 □L Formaldehyde in 100 mL of demineralized water) was next added to the gels on a shaker for 20 minutes. The gels were quickly rinsed twice with

dH_2O. The developer solution (2 g Sodium Carbonate, 20-40 □L formaldehyde, 5 mL of staining activator in 100 mL of demineralized water) was added and observed closely while the image developed. At the appropriate time, the developer was discarded and rinsed quickly with dH_2O, and the stop solution (5% acetic acid) was added for 2 minutes. The stop solution was rinsed 3 times and the gels imaged on a G:BOX Chemi (SynGene; XRQ).

2.8 Electron Microscopy

Sample purity was evaluated by negative staining of the fractions using transmission electron microscopy (TEM). Briefly, purified HCoV-OC43 fractions 6 and 17 were inactivated using 0.8 % of paraformaldehyde for 30 minutes at 4°C. The inactivated samples were deposited on square 200-mesh Formvar carbonated copper-coated grids (Electron Microscopy Sciences; FCF200-Cu-50). Excess liquid was blotted away with filter paper, and the samples were stained for contrast with 2% uranyl acetate (Canemco and Marivac). The grids were then washed in 1M HEPES buffer (Sigma; 83264; PH: 7.0-7.6) and dried on filter paper. Samples were examined with Philips Tecnai 12 Transmission Electron Microscope.

2.9 Mass spectrometry

The protein concentration of the Optiprep fractions 6 and 17 was quantified using the Pierce BCA Protein Assay Kit (Thermo Fisher). Ten micrograms of the purified fractions 6 (as an exosome fractions) and fraction 17 (as virus fractions) from both mock-infected and HCoV-OC43 infected samples were inactivated by heating 1h at 80°C and sent to the proteomics platform of the Institute for Research in Immunology and Cancer (IRIC) with special thanks to Dr. Éric Bonneil.

There, samples were reconstituted in 50 mM ammonium bicarbonate with 10 mM TCEP [Tris(2-carboxyethyl)phosphine hydrochloride; Thermo Fisher Scientific], and vortexed for 1 h at 37°C. For alkylation Chloroacetamide (Sigma-Aldrich; final concentration of 55 mM) was added. Samples were vortexed for another hour at 37°C. Digestion step was started by adding One microgram of trypsin for 8 h at 37°C. Samples were dried down and solubilized in 5% ACN(Acetonitrile) -4% formic acid (FA). Then samples were loaded on a 1.5 µl pre-column (Optimize Technologies, Oregon City, OR). Peptides were separated on a home-made reversed-phase

column (150-µm i.d. by 200 mm) with a 56-min gradient from 10 to 30% ACN-0.2% FA and a 600-nl/min flow rate on an Easy nLC-1200 connected to a Exploris 480 (Thermo Fisher Scientific, San Jose, CA). Each full MS spectrum acquired at a resolution of 120,000 was followed by tandem-MS (MS-MS) spectra acquisition on the most abundant multiply charged precursor ions for 3s. Tandem-MS experiments were performed using higher energy collision dissociation (HCD) at a collision energy of 34%. The data were processed using PEAKS X Pro (Bioinformatics Solutions, Waterloo, ON) and a concatenated database made of Uniprot human (20349 entries) and HCOV-OC43 (22 entries) databases. Mass tolerances on precursor and fragment ions were 10 ppm and 0.01 Da, respectively. Fixed modification was carbamidomethyl (C). Variable selected posttranslational modifications were acetylation (N-ter), oxidation (M), deamidation (NQ), phosphorylation (STY). The data were visualized with Scaffold 5.0 (95% protein and peptide thresholds; minimum of 2 peptides identified; false-discovery rate [FDR] of 1% for peptides; reproductible in all three independent replicates).

2.10 Viability Assay

Twenty-four hours before the viability test, HRT-18 cells were seeded in 96-well Greiner black plates. One hour before transfection, fresh Optipro media was added to all wells. The cells were treated with 100 nM of either control dsiRNA (NC1) or 19 dsiRNAs targeting the host proteins (14 dsiRNAs targeting host proteins from virus fraction and 5 dsiRNAs targeting exosome fraction hits) using the LipoJet siRNA transfection kit (SignaGen #SL100468). The dsiRNAs and their targets are listed in Table1. We monitored cellular activity 72h post-transfection by adding 10% alamarBlue (Invitrogen; DAL1025) to the wells for three hours at 37°C. Fluorescence intensity was measured using a BMG Labtech Clariostar microplate reader at 560nm and 590nm. All wells were normalized to a non-transfected control.

Table 1. Down-regulation of cellular proteins by dsiRNAs

	DsiRNAs targeting virus fraction proteins (100 nM)	DsiRNAs targeting exosome fraction proteins (100 nM)
1	dsi-IMPAD	dsi-CLU
2	dsi-MOV10	dsi-DARS1
3	dsi-MFGE8	dsi-TSPAN15
4	dsi-PABPC1	dsi-EIF3C
5	dsi-PRSS2	dsi-GSTM3
6	dsi-RAB2A	
7	dsi-RAB6A	
8	dsi-SCYL1	
9	dsi-TINAGL1	
10	dsi-DDX1	
11	dsi-PABPC4	
12	dsi-PPP1CB	
13	dsi-RAB7A	
14	dsi-SYNCRIP	

A poll of two dsiRNAs (*except for PRSS2 which has only one dsiRNA) was designed and synthesized by IDT DNA for each target. HRT-18 cells were transfected with 100 nM of dsiRNAs, and 72 hours post-transfection, cells activity was measured by using 10% alamarBlue reagent.*

2.11 DsiRNA knock-down

A total of 170,000 HRT-18 cells per well were seeded in 12-well plates 24 hours before transfection. One hour before transfection, the media was changed with Optipro SFM media. Transfection was done with 100nM dsiRNAs with a poll of two distinct dsiRNAs for each target, except for PRSS2 which has only one dsiRNA using the LipoJet siRNA transfection kit (SignaGen

#SL100468).Twenty-four hours after transfection, HRT-18 transfected cells were infected with HCoV-OC43 with MOI of 0.1 and treated with Optipro media. Forty-eight hours post-infection (total 72 hours of dsiRNA transfection), the whole cell lysate was collected in 200 µl of PBS in a 1.5 ml Eppendorf tube, centrifuged for 10 minutes at 315g at 4°C. The pellet was resuspended in 25µl of MNT Buffer (30 mM MES, 100 mM NaCl, 20 mM Tris-HCl, pH 7.4), followed by 4 cycles of freeze and thaw in liquid nitrogen and 37°C water to break up the cells. The tubes were sonicated 15 times for 1 second at intensity 8 ,then snap-frozen in liquid nitrogen and stored at -80°C. The virus titration was performed with $TCID_{50}$/ml-IPA. A non-targeting control, NC1 (IDT DNA; 51-01-14-04), was used as a transfection reference. A fluorescent oligonucleotide duplex marker, SiGLO (horizon discovery; D-001630-01-05), was used to verify transfection success. The GFP green, fluorescent signal for SiGLO and was checked with a Leica DMi8 inverted wide-field fluorescence microscope.

2.12 SARS-CoV-2 samples

The inactivated SARS-CoV-2 samples were prepared at the CHUM research center in collaboration with Dr.Nathalie Grandvaux's lab. The delta SARS-CoV-2 was produced in Vero-E6 cells, the supernatant was collected and inactivated using 0.05% β-Propiolactone for 16h at 4°C followed by 2h at 37°C. Complete viral inactivation was validated by the $TCID_{50}$ method. The inactivated SARS-CoV-2 and Mock samples were concentrated using Amicon 100-kDa filter, same as for HCoV-OC43 virions. One ml of the concentrated sample was next loaded on top of the above-described Optiprep/sucrose continues gradient and ultracentrifuged in a Hitachi (CP-100NX) P40ST rotor at 250,000 G for 135 min. Eighteen fractions were collected from the top to the bottom of the gradient for SARS-CoV-2 infected as well as mock-infected samples.

Equal volumes (50 µl) of all fractions were mixed with 5X loading buffer and heated at 95°C for 5 minutes. Samples were then loaded on 5 to 20% SDS-PAGE gradient gels. The details of Western blot reagents and antibodies are described in section 2.5.

Chapter 3—Results

3.1 HRT-18 cells express the CD9 and CD63 Exosome Markers

The main purpose of the project is to delineate the coronavirus-incorporated host proteins to ultimately decipher their role in the coronaviral life cycle. We first aimed to purify HCoV-OC43 extracellular virions as proof of concept since they are easier to work with (biosafety level 2) , with the intention to later study SARS-CoV-2. However, it was important to define which exosomes are produced by the infected cells. We choose the HRT-18 cell line for HCoV-OC43 infection and production for several reasons. First, our lab previously studied the spread of the virus in different cell lines and found that the HRT-18 and MRC-5 cell lines had the highest viral yields (110). Since HRT-18 cells grow faster than MRC-5 cells and as we needed sufficient virus for downstream MS analysis, the HRT-18 cell line was determined to be the best option. Secondly, the HRT-18 is a human cell line, which was convenient and relevant for our MS analyses. However, we did not originally know about their exosome profile, an important aspect to select the best purification protocol. In the first step, we therefore checked by Western blotting the exosome profile in the HRT-18 cell line produced in serum free conditions to limit exogenous exosomes coming from serum (112). Immunoblots against the classical exosome markers CD9, CD63 and CD81 using mock and HCoV-OC43 total cell lysates showed that we could detect CD9 and CD63 in mock-infected and HCoV-OC43 infected samples (Figure 14). In addition, the CD9 marker was detectable in the media and ultracentrifugation pellets of that media in both mock and HCoV-OC43 infected samples. This indicated that HRT-18 cells are CD9 and CD63 positive but only secrete detectable CD9 containing exosomes that were enriched by centrifugation. Moreover, the virus did not appear to modulate CD9 and CD63, as their expression levels and molecular weights showed no apparent change in HCoV-OC43-infected samples compared to mock cells. In contrast, we could not detect any evidence of the CD81 exosome marker in HRT-18 cells, neither in mock nor in HCoV-OC43 infected cells.

In the next step we checked the presence of exosome markers in Vero-E6 cells. Vero-E6 is the cell line routinely used for production of SARS-CoV-2 samples, which will prove useful later on.

Western blot results showed that the Vero-E6 cell line expresses all three exosome markers, albeit they it did not appear to release them in detectable amounts in the tissue culture media (Figure 15). Nonetheless, this reaffirmed that the pattern of exosome markers can vary between cell lines, confirmed that the CD81 antibody worked well and that HRT-18 cells do not produce detectable levels of CD81.

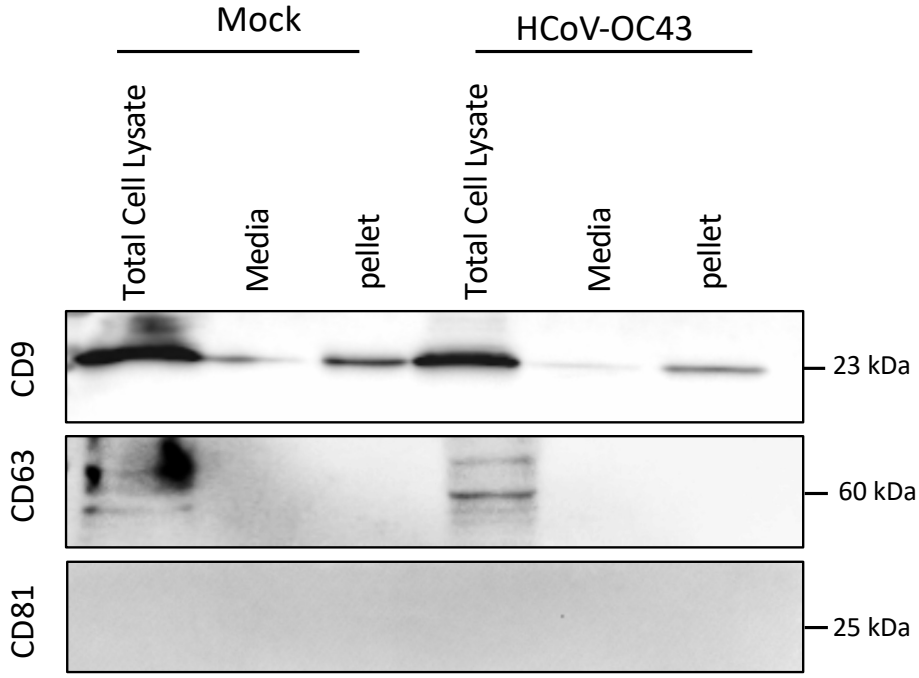

Figure 14. Expression of exosome markers in HRT-18 cells

HRT-18 cells were infected with the HCoV-OC43 VR1558 virus. After one-hour absorption, the SFM Optipro media were added to the viruses. Three DPI, the media was collected, filtered with a 0.4 µm filter, and ultracentrifuged at 100,000 x g for 1h. Total cell lysate, *0.4 µm filtered media and pellet were immune blotted for exosome specific markers CD9, CD63, and CD81 for both Mock and HCoV-OC43 Infected samples (n=3).*

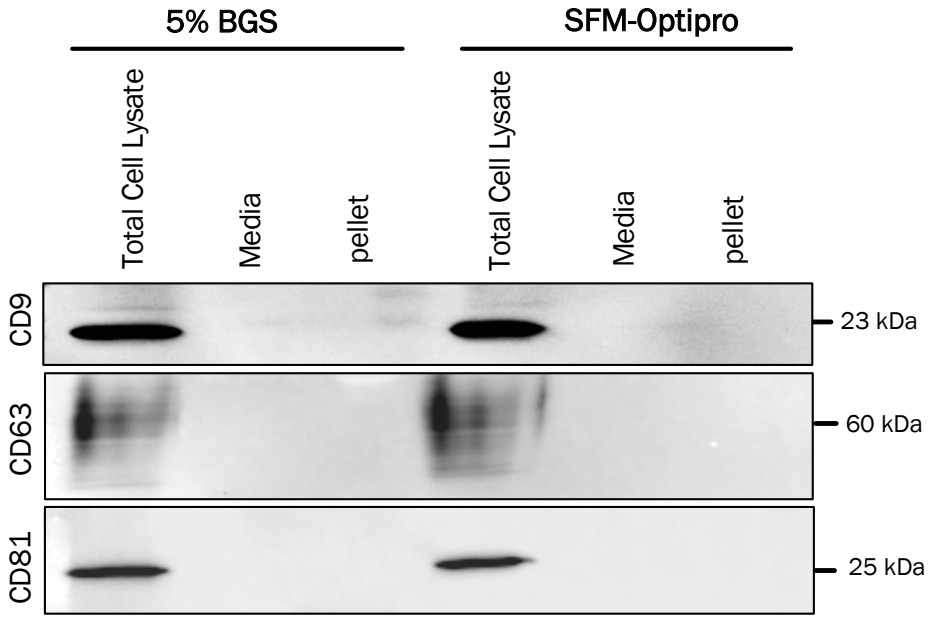

Figure 15. Expression of exosome markers in Vero-E6 cells

Vero-E6 cells were incubated with SFM Optipro media or DMEM with 5% Bovine Growth Serum for 24 h. After that, the media was collected, filtered with 0.4 µm and ultracentrifuged at 100,000 x g for 1h. Total cell lysate, *0.4 µm filtered media and pellet, were immunoblotted for exosome specific markers CD9, CD63, and (n=3).*

3.2 The Optiprep Density Gradient is an Optimal Method to Concentrate Coronavirions

Concentrating extracellular viruses is both required for MS analyses and an opportunity to reducing extracellular contaminants. To this end, we tested two methods for virus concentration: **a)** Amicon filtration with a large cut off (100 kDa) that prevents the passage of the virus through the filter while letting most other components through and **b)** Ultracentrifugation at different forces to separate virions from other large particles. Samples from each step were collected and the titer of viruses in each step was quantified using the $TCID_{50}$-IPA method (110). Our results (Table 2) indicated that Amicon filtration augmented viral titers by 29 times while recovering

48.2% of all virions. For ultracentrifugation, the concentration of infectious particles was at best 16 times greater than in the original media and the total recovery 32%. In conclusion, the Amicon filtration showed more promising results in virus concentration and final recovery of the virus and was used in subsequent steps of our proteomics protocol.

Table 2. Concentration and total recovery of extracellular virus concentration methods

Method	Sample	Volume	$TCID_{50}$/ml (Mean±SEM)	Concentration (X)	Total Recovery (%)
Amicon filter	Media	3x 60 ml	3.01 E+08 ± 1.65E+08	1	100
	0.4 µm Filter media	3x 60 ml	3.54 E+08 ± 1.46E+08	1.2	117.5
	Amicon filter	3ml	8.75 E+09 ± 2.43E+09	29.0	48.2
Ultracentrifugation	Media	10 ml	8,75 E+07 ± 2.43E+07	1	100,0
	0.4 µm Filter media	10 ml	8,75 E+07 ± 2.43E+07	1,0	100,0
	Pellet 20K xg	0.2 ml	3.01 E+08 ± 1.65E+08	3.4	6.9
	Pellet 60K xg	0.2 ml	5.19 E+08 ± 1.13E+08	5.9	11.9
	Pellet 100K xg	0.2 ml	1.40 E+09 ± 7.69E+08	16.0	32.0

$TCID_{50}$ using DAB staining ($TCID_{50}$/ml-IPA) were done to calculate concentration and total recovery of each step during virus concentration: The media of infected cells, media after filter using 0.4 µm filter, concentrated media with Amicon filter and pellet after ultracentrifugation. (n=3)

3.3 Efficient Separation of Extracellular Virions from Exosomes

After concentrating the viruses using Amicon filtration, we needed to employ a method to separate exosomes from HCoV-OC43 virions. HCoV-OC43 is around 80 nm and exosomes are 30-150 nm (113). Therefore, by concentrating the virus, we would likely also concentrate the exosomes. Interestingly, Dogrammatzis C et al had previously shown that they could successfully achieve the separation of HSV-1 viral particles from exosomes on an iodixanol (Optiprep) density gradient (109). We therefore postulated such a gradient might also separate HCoV-OC43 and exosomes. Amicon concentrated virus or control mock-infected samples were therefore loaded on the top of the Optiprep/sucrose density gradient. Eighteen fractions were collected from the top (fraction 1) to the bottom (fraction 18) of the gradient. Fractions were analyzed by Western blotting using antibodies against the N viral protein and the CD9 and CD63 exosome markers. Figure 16A shows that for the HCoV-OC43 infected samples, the viral N protein was highly enriched in fractions 16 to 18, while exosomes were mainly present in fractions 4 to 13, with traces across the gradient. In mock infected samples, the viral N protein was not detectable in any fraction, which validated the specificity of the N antibody towards viral proteins. Interestingly, exosomes from non-infected cells were present in the same fractions as HCoV-OC43 infected fractions. This revealed two points: first, there was no significant change in the overall level of exosome expression, and second, the pattern of exosome distribution between mock and HCoV-OC43 infected fractions was essentially the same. This suggested that the HCoV-OC43 virus did not affect the exosome expression levels, nor grossly alters their properties.

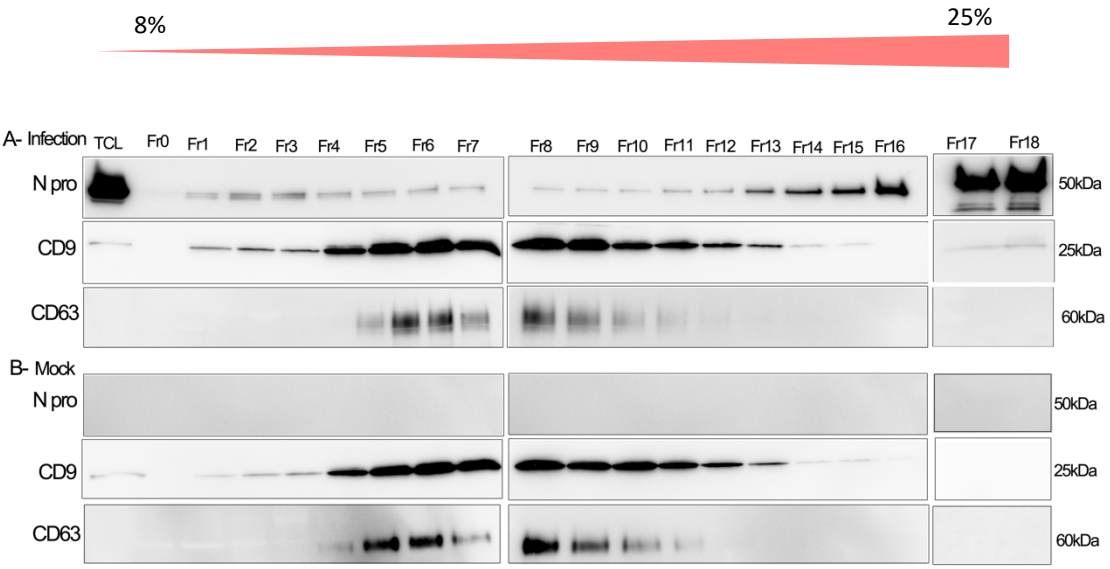

Figure 16. Separation of exosomes and virus after fractionation

HRT-18 cells were mock-infected or virus-infected with the HCoV-OC43 VR1558 virus and treated with SFM Optipro media. Three DPI, the supernatant was collected, filtered with 0.4 µm filter, and then concentrated using 100 kDa Amicon Millipore filter. The sample was then loaded on top of a continuous Optiprep/sucrose gradient ranging from 8 to 25%. Samples were ultracentrifuged for 135 min at 250,000 × g at 4°C. Eighteen fractions were collected from the top (fraction 1) to the bottom (fraction 18) of the gradient using a hydraulic pump. Fifty microliters of each fraction and total cell lysate (TCL) were mixed with 5x sample buffer, heated for 5 min at 95°C, and loaded on a 5–20% gradient SDS gel. The separation of exosome markers and virus in each fraction was checked using antibodies against exosome markers CD9 and CD63 and N protein of HCoV-OC43, ***16-A*** *shows the fractions from HCoV-OC43 fractions and* ***16-B*** *shows fractions from mock HRT-18 cells(n=3).*

3.4 Infectious HCoV-OC43 Particles Overlap with the Viral N Protein Marker Along the Density Gradient

By using WB against the HCoV-OC43 N protein, we detected the presence and enrichment of HCoV-OC43 N protein in the higher densities of the Optiprep gradient. To ensure that we were collecting intact infectious particles and not just cellular membranes containing the N protein, we quantified the infectious particles in these fractions. Figure 17 shows that the virus titer was maximal at fraction 17. These results are consistent with our WB results as fraction 17 has the most enriched viral particles with a titer of 10^9 $TCID_{50}$/ml. We therefore selected fraction 17 as the "virus fraction" for MS analysis, since it had the highest proportion of infectious particles and the least exosome markers. Furthermore, we choose fraction 6 for further MS analysis as an "exosome fraction", as it exhibited good expression levels of CD9 and CD63 exosome markers in both mock and virus-infected fractions and no evidence for intact virions in the mock.

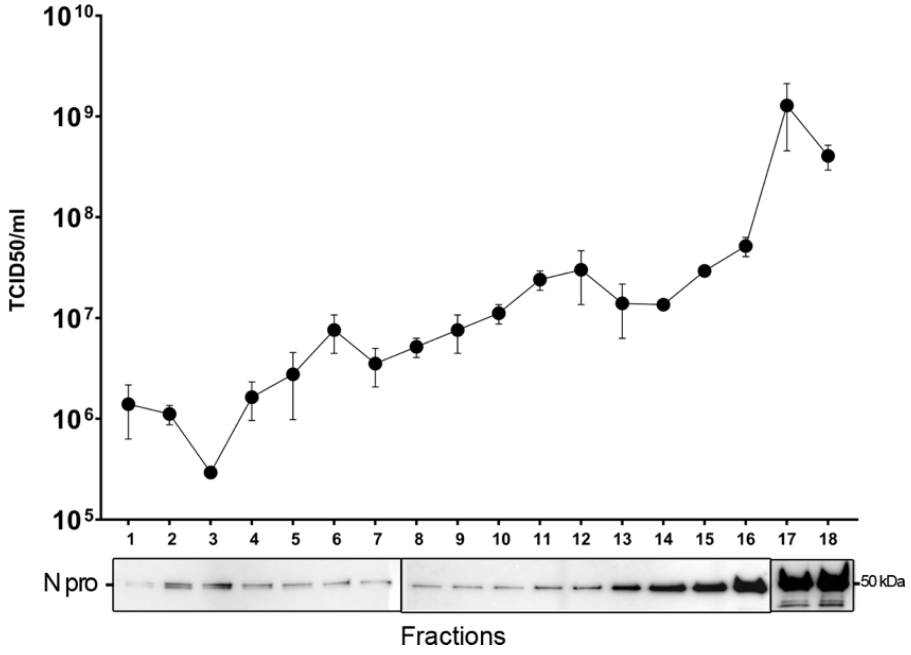

Figure 17. $TCID_{50}$/ml-IPA on HCoV-OC43 fractions

HRT-18 cells were cultured in 96-well plates, infected with the serial dilution of HCoV-OC43 fractions collected from the above Optiprep density gradient. The primary antibody used in the $TCID_{50}$/ml assay targets the HCoV-OC43 S protein. For the western

blot, fifty microliters of each fraction were mixed with 5x sample buffer, heated for five mins at 95°C, and loaded on a 5–20% gradient SDS gel and blotted for the N protein of HCoV-OC43 (n=3).

3.5 Fractions 6 and 17 Are Strongly Enriched for Intact Exosomes and Virions

As sample purity is critical for MS, both the viral and exosome fractions were additionally monitored by silver staining. Fifty microliters of exosomes (fraction 6) or virus (fraction 17) derived from HCoV-OC43, or control mock-infected cells were thus loaded on SDS gels and stained as detailed in the Materials and Methods section. As anticipated, the data revealed distinct protein patterns between the exosome and viral samples in agreement with our previous WB results (Figure 18). In addition, there was a strong enrichment for both viral and exosome markers in their respective samples. For instance, strong bands corresponding to the viral N (50 kDa), S (before glycosylation, the S protein has a molecular mass of 120-160 kDa, and after glycosylation, this increases up to 150-200 kDa (39)), M (25 kDa) and HE (50-75 kDa (114)) were apparent in fraction 17 of infected cells but not in mock fraction. Similarly, tetraspanin exosome markers CD9 (23 kDa) and CD63 (60 kDa) could be detected in fraction 6 derived from both mock and infected cells. Interestingly, there was a near complete lack of proteins in the mock fraction 17, suggesting there were very few if any contaminants in the viral fraction. In addition, there was clear indication that the protein content of the exosomes is altered by the virus as the band patterns differed between fractions 6 from mock or infected cells.

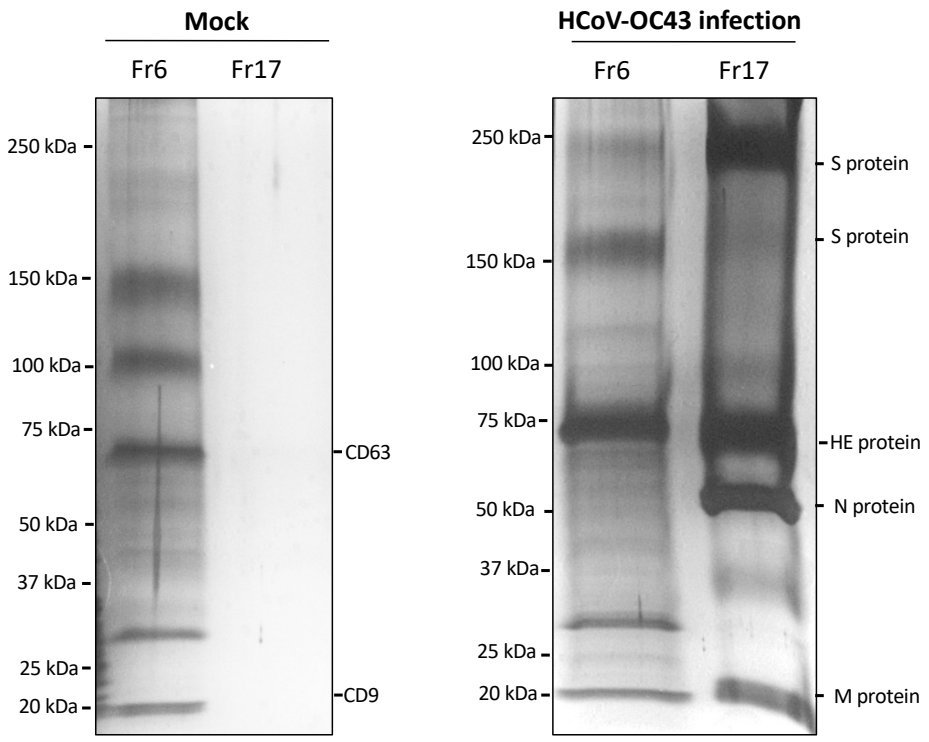

Figure 18. Silver staining of mock and HCoV-OC43- infected fractions

Extracellular mock and HCoV-OC43 infected fraction loaded on the 5-20% SDS gradient gel and stained. The viral S (different molecular weighs due to different glycosylation*), N, M HE, and exosomes markers CD9 and CD63 with predicted molecular weights on the right side and the molecular weights on the left side can be detected in the blot.*

We next evaluated the purity and integrity of the viral particles and exosomes by electron microscopy. However, we needed to first inactivate the HCoV-OC3 virus (biosafety level 2) to take them to the microscope. Since paraformaldehyde (PFA) efficiently crosslinks proteins, we looked for the lowest concentration of PFA that could inactivate HCoV-OC43. We tried different concentrations of PFA from 0.1 % up to 4% at 4°C for 30 minutes, 1 hour and 2 hours. After each treatment, viral titers were quantified by $TCID_{50}$ along with non-inactivated virus as control. The mean titer of untreated virus was 3.37E+08 ± 1.64E+08 (mean ± SEM of three independent experiments) , which was considered the 100% mark. The results of PFA inactivated samples are

shown in Figure 19. The data shows that PFA efficiently killed the virus in a dose-dependent fashion. For biosafety reasons, we chose to treat our samples with 0.8% PFA for 30 minutes to completely inactivate the virus prior to loading them on EM grids to check the fractions using TEM.

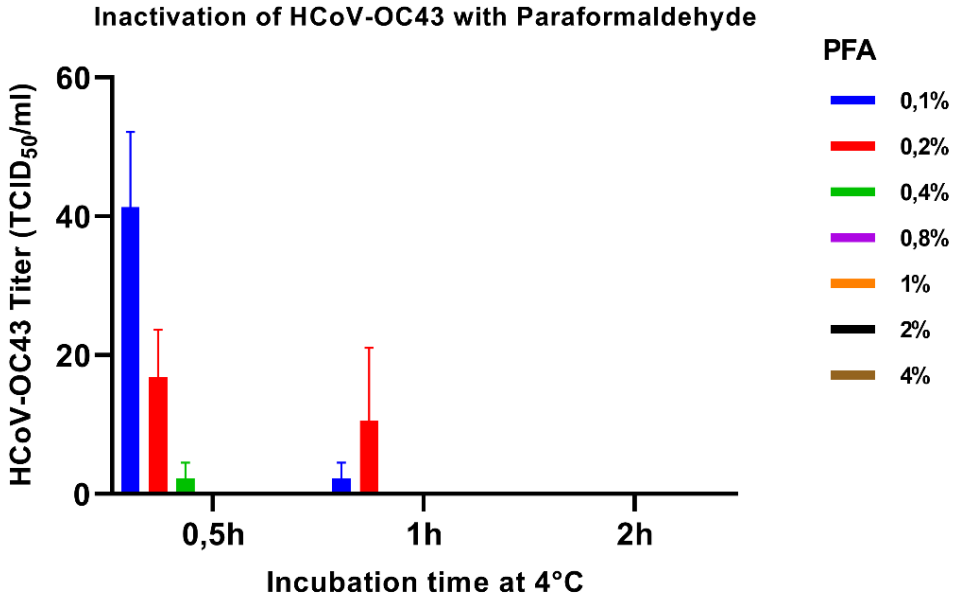

Figure 19. Inactivation of HCoV-OC43 using paraformaldehyde

Various concentrations of PFA from 0.1 % up to 4% were used to check HCoV-OC43 titration after inactivation for 30 minutes, 1 hour and 2 hours at 4°C. The virus titration was done using $TCID_{50}$/ml-IPA.

Analysis of the inactivated samples by TEM showed that the mean size of 19 particles measured in the virus fraction was 78.9±1.47 (mean ± SEM) (Figure 20) which is compatible with the HCoV-OC43 particle size (38). The particle sizes in the exosome for mock (Figure 20) and HCoV-OC43 infected fraction were 33.2±1.04 nm and 36.4±1.9 nm respectively (mean ± SEM), which was significantly smaller ($P<0.05$) than the virus despite their reported size, which varies from 30 to 100 nm (89). Statistical significance was determined using the T-test with 95% confidence interval. Most importantly, the samples were very clean and devoid of cell debris/contaminants or cross contamination between the virus and exosomes.

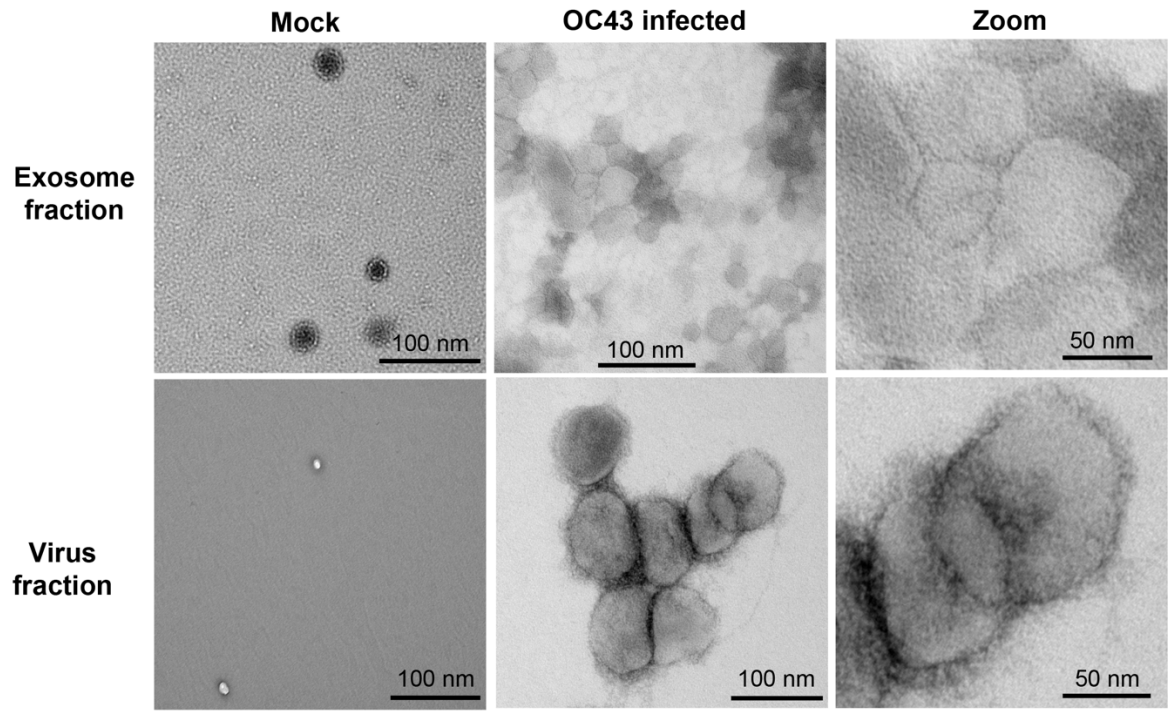

Figure 20. TEM images from exosome and virus fractions

Mock and HCoV-OC43 exosome and virus fractions, inactivated with 0.8% PFA, deposited on Formvar carbonated copper-coated grids, stained with 2% uranyl acetate, and examined by TEM .

3.7 Mass spectrometry

3.7.1 Fraction 17 from Infected Cells Is Strongly Enriched in Virions

Ten micrograms of exosome and virus fractions (fractions 6 and 17) of mock and HCoV-OC43 infected samples from 3 independent experiments were injected into a LC-MS/MS spectrometer. The protein content of fractions was identified using a human and HCOV-OC43 combined database. The MS raw data was first analyzed with PEAKS X Pro to identify the peptides, then further processed with Scaffold to visualize the data considering three parameters: 1) the presence of the protein in all independent triplicates; 2) a minimal spectral count of two; 3) 95% confidence thresholds for both proteins and peptides. Under these conditions, we detected four virus structural proteins N, S, M, and HE in the HCoV-OC43 infected fractions but not in the mock samples (Table3). Unexpectedly, we were unable to detect the envelope protein. One explanation might be that it remains stuck in the LC column. Moreover, few of these molecules may be assembled into mature viral envelopes (115). This is corroborated by Zeng et al. who reported that they did not find E protein in their MS analysis either (57, 106). Albeit there were traces of viral proteins in the exosome fraction derived from infected cells, they were highly enriched in the viral fraction (16, 21, 43, and 17 times more abundant than that of the exosome fraction for N, S, M, and HE proteins respectively; Table 3), which confirms our previous WB and $TCID_{50}$/ml results (Figures 14 and 15). We also found no exosome markers in the virus fraction, confirming the quality of our separation method. Moreover, exosome fractions confirmed the presence of the exosome markers in agreement with the WB results.

Table 3. HCoV-OC43 structural proteins enrichment in virus-infected fractions

Sample	HCoV-OC43 Protein	Fold enrichment (fr17/fr6)
Mock fraction 6	n/a	n/a
Mock fraction 17	n/a	n/a
HCoV-OC43 fraction 6	Hemagglutinin-esterase	1
	Nucleoprotein	1
	Spike glycoprotein	1
	Membrane protein	1
HCoV-OC43 fraction 17	Hemagglutinin-esterase	17.4
	Nucleoprotein	16
	Spike glycoprotein	21.2
	Membrane protein	41.3

The average of MS total spectra (3 independent experiments) was used to calculate the enrichment of viral particles in the virus-infected fraction 17 compared to the virus-infected exosome fraction 6. Note that viral proteins were not detected in the mock-infected fractions used as a control (n/a: not applicable).

3.7.2 The Extracellular Virions and Exosomes Contain Several Unique Proteins

The overall cellular protein content of mock and HCoV-OC43 infected fractions identified by MS are shown in a Venn diagram (Figure 21). For the virions, 18 different cellular proteins found in the viral sample (fraction 17 from infected cells) were also identified in the control (fraction 17 from non-infected cells). To limit potential contaminants, these proteins were removed from our final list, giving us 69 unique cellular proteins incorporated into the virus (these host proteins are listed in Table 4).

For exosomes (fractions 6), 176 proteins were common between mock and HCoV-OC43 infected, while 49 proteins were unique to the HCoV-OC43 infected exosome fraction (Figure 21B). In contrast, 97 proteins were unique to exosomes derived from non-infected cells, suggesting that

the virus altered the composition of these exosomes, as indicated by the above silver staining data.

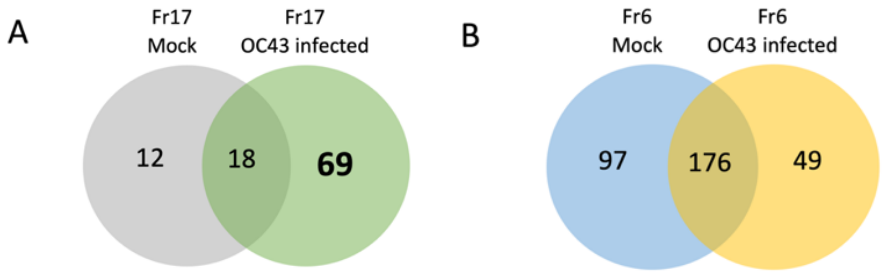

Figure 21. Cellular protein content of virus and exosome fractions

*The Venn diagrams show the number of distinct cellular proteins identified by mass spectrometry in the **A)** viruses (fractions 17) or **B)** exosomes (fractions 6). As above, a threshold of 95% protein and peptide probabilities and a minimum of 2 peptides were applied.*

To define the most relevant proteins, we analyzed our Scaffold data with PANTHER (protein analysis through evolutionary relationships). This software allows us to determine the main pathways along which the identified protein act. It revealed RNA metabolic pathways (13% of all identified proteins) are overrepresented among the host proteins incorporated in the virus, followed by metabolite interconversion (10%), protein modifying enzymes (9%) and protein-binding activity modulator (9%) (Figure 22 and Table 4). Similarly, among the 49 unique proteins found in HCoV-OC43 infected exosome fraction, translational proteins account for 16% of the total proteins followed by metabolite interconversion enzyme (14%) and scaffold protein (6%) (Figure 23 and Table 5).

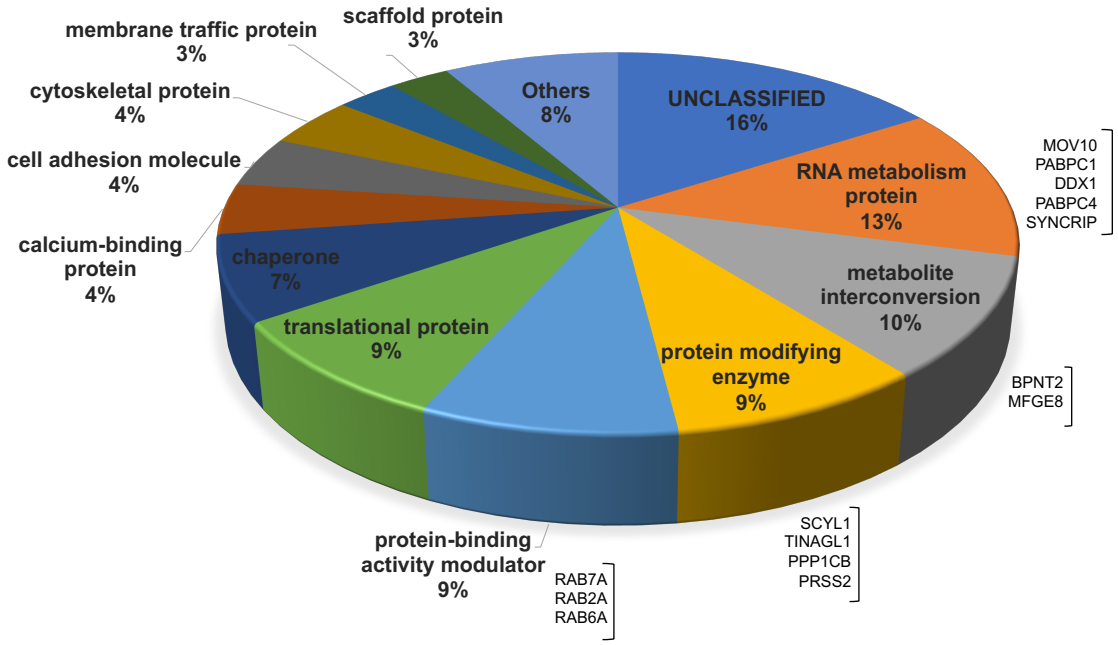

Figure 22. Distribution of cellular protein pathways associated with the virus

The pie chart shows the protein pathways of 69 unique cellular proteins found in purified extracellular viruses.

Table 4. Unique cellular proteins associated with HCoV-OC43 infected virus fraction

	Protein ID	Accession number	Orthologs	Protein class
1	AGRN	O00468	Agrin	cell adhesion molecule
2	ALDOA	P04075	Fructose-bisphosphate aldolase	aldolase
3	ANXA11	P50995	Annexin A11	Calcium-binding protein
4	ANXA2	P07355	Annexin A2	Calcium-binding protein
5	ARF1	P84077	ADP-ribosylation factor 1	G-protein
6	ARF4	P18085	ADP-ribosylation factor 4	G-protein
7	BPNT2	Q9NX62	Golgi-resident adenosine 3',5'-bisphosphate	Phosphatase
8	CALM2	P0DP24	Calmodulin-2	calmodulin-related
9	CFL1	P23528	Cofilin-1	non-motor actin binding protein
10	DDX1	Q92499	ATP-dependent RNA helicase DDX1	RNA helicase
11	DDX3X	O00571	ATP-dependent RNA helicase DDX3X	RNA helicase
12	DNAJA1	P31689	DnaJ homolog subfamily A member 1	chaperone
13	DNAJA2	O60884	DnaJ homolog subfamily A member 2	chaperone
14	EEF2	P13639	Elongation factor 2	translation elongation factor
15	EIF4A1	P60842	Eukaryotic initiation factor 4A-I	RNA helicase
16	EIF4H	Q15056	Eukaryotic translation initiation factor 4H	translation initiation factor
17	EIF5A	P63241	Eukaryotic translation initiation factor 5A-1	translation initiation factor

18	ENO1	P06733	Alpha-enolase	lyase
19	FAM3C	Q92520	Protein FAM3C	antimicrobial response protein
20	FAM98A	Q8NCA5	Protein FAM98A	RNA splicing factor
21	GDF15	Q99988	Growth/differentiation factor 15	growth factor
22	GIPC1	O14908	PDZ domain-containing protein GIPC1	scaffold/adaptor protein
23	GORASP2	Q9H8Y8	Golgi reassembly-stacking protein 2	unclassified
24	GPC1	P35052	Glypican-1	scaffold/adaptor protein
25	HSP90AA1	P07900	Heat shock protein HSP 90-alpha	Hsp90 family chaperone
26	HSPA1A	P0DMV8	Heat shock 70 kDa protein 1A	Hsp70 family chaperone
27	HSPD1	P10809	60 kDa heat shock protein, mitochondrial	unclassified
28	HSPG2	P98160	Basement membrane-specific heparan sulfate proteoglycan core protein	immunoglobulin superfamily cell adhesion molecule
29	KRT2	P35908	Keratin, type II cytoskeletal 2 epidermal	unclassified
30	KRT8	P05787	Keratin, type II cytoskeletal 8	unclassified
31	LGALS3	P17931	Galectin-3	extracellular matrix protein
32	MFGE8	Q08431	Lactadherin	oxidoreductase
33	MOV10	Q9HCE1	Helicase MOV-10	RNA helicase
34	MYOF	Q9NZM1	Myoferlin	unclassified
35	NAP1L1	P55209	Nucleosome assembly protein 1-like 1	chromatin/chromatin-binding
36	NME1	P15531	Nucleoside diphosphate kinase A	kinase
37	PABPC1	P11940	Polyadenylate-binding protein 1	RNA metabolism protein

38	PABPC4	Q13310	Polyadenylate-binding protein 4	RNA metabolism protein
39	PCBP1	Q15365	Poly(rC)-binding protein 1	RNA metabolism protein
40	PEX5	P50542	Peroxisomal targeting signal 1 receptor	membrane trafficking regulatory protein
41	PFN1	P07737	Profilin-1	non-motor actin-binding protein
42	PPIA	P62937	Peptidyl-prolyl cis-trans isomerase A	chaperone
43	PPP1CA	P62136	Serine/threonine-protein phosphatase PP1-alpha catalytic subunit	protein phosphatase
44	PPP1CB	P62140	Serine/threonine-protein phosphatase PP1-beta catalytic subunit	protein phosphatase
45	PRDX1	Q06830	Peroxiredoxin-1	peroxidase
46	PRSS2	P07478	Trypsin-2	serine protease
47	RAB21	Q9UL25	Ras-related protein Rab-21	Small GTPase
48	RAB2A	P61019	Ras-related protein Rab-2A	Small GTPase
49	RAB6A	P20340	Ras-related protein Rab-6A	Small GTPase
50	RAB7A	P51149	Ras-related protein Rab-7a	Small GTPase
51	RPL11	P62913	60S ribosomal protein L11	Ribosomal protein
52	RPS12	P25398	40S ribosomal protein S12	Ribosomal protein
53	RPS4X	P62701	40S ribosomal protein S4, X isoform	Ribosomal protein
54	RTCB	Q9Y3I0	RNA-splicing ligase RtcB homolog	unclassified
55	RTRAF	Q9Y224	RNA transcription, translation, and transport factor protein	unclassified

56	SCYL1	Q96KG9	N-terminal kinase-like protein	non-receptor serine/threonine protein kinase
57	SDC4	P31431	Syndecan-4	transmembrane signal receptor
58	SDCBP	O00560	Syntenin-1	membrane trafficking regulatory protein
59	SLC12A2	P55011	Solute carrier family 12-member 2	secondary carrier transporter
60	SYNCRIP	O60506	Heterogeneous nuclear ribonucleoprotein	RNA metabolism protein
61	THBS1	P07996	Thrombospondin-1	cell adhesion molecule
62	TINAGL1	Q9GZM7	Tubulointerstitial nephritis antigen-like	cysteine protease
63	TRIM26	Q12899	Tripartite motif-containing protein 26	ubiquitin-protein ligase
64	TRIM32	Q13049	E3 ubiquitin-protein ligase TRIM32	unclassified
65	TUBB	P07437	Tubulin beta chain	tubulin
66	TXN	P10599	Thioredoxin;TXN	oxidoreductase
67	YBX1	P67809	Y-box-binding protein 1;YBX1	
68	YBX3	P16989	Y-box-binding protein 3	unclassified
69	ZC3HAV1	Q7Z2W4	Zinc finger CCCH-type antiviral protein	unclassified

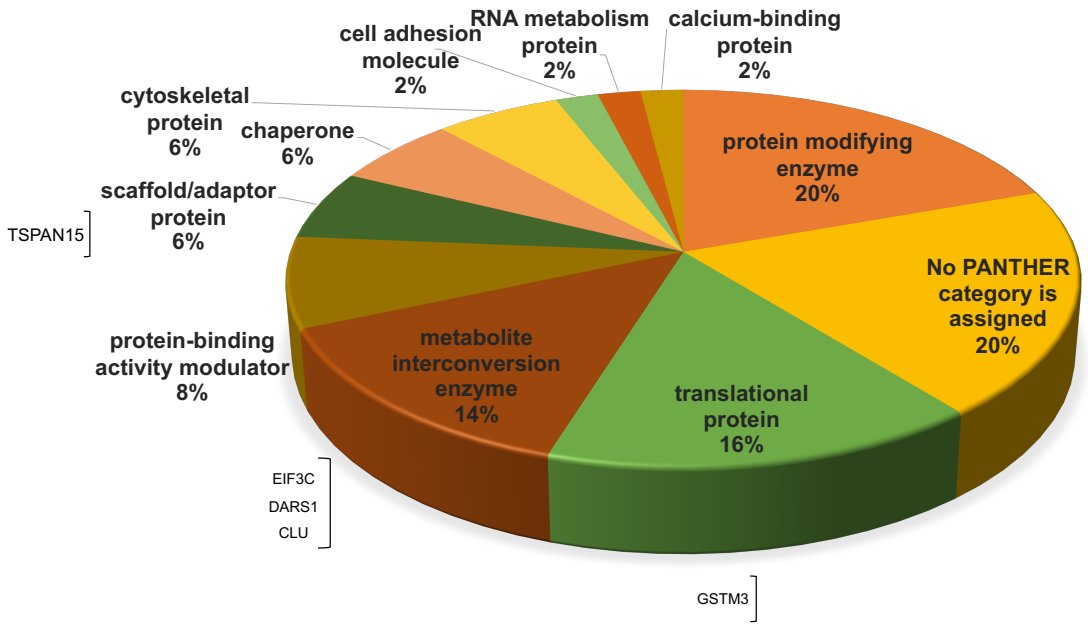

Figure 23. Distribution of cellular protein pathways associated with exosome fraction

The pie chart shows the protein pathways of 49 unique cellular proteins found in the HCoV-OC43 infected exosome fraction.

Table 5. Unique cellular proteins associated with HCoV-OC43 infected exosome fraction

	Protein ID	Accession number	Orthologs	Pathways
1	ACTN1	P12814	Alpha-actinin-1	cytoskeletal protein
2	ACTR2	P61160	Actin-related protein 2	cytoskeletal protein
3	AHCY	P23526	Adenosylhomocysteinase	metabolite interconversion enzyme
4	ANXA3	P12429	Annexin A3	calcium-binding protein
5	ARF4	P18085	ADP-ribosylation factor 4 OS=Homo sapiens	protein-binding activity modulator
6	CALR	P27797	Calreticulin	chaperone
7	CAND1	Q86VP6	Cullin-associated NEDD8-dissociated protein 1	protein modifying enzyme
8	CD59	P13987	CD59 glycoprotein	Unclassified
9	CLU	P10909	Clusterin	translational protein
10	DAG1	Q14118	Dystroglycan 1	Unclassified
11	DARS1	P14868	Aspartate-tRNA ligase, cytoplasmic	translational protein
12	EEF1G	P26641	Elongation factor 1-gamma	Unclassified
13	EIF3B	P55884	Eukaryotic translation initiation factor 3 subunit B	translational protein
14	EIF3C	Q99613	Eukaryotic translation initiation factor 3 subunit C	translational protein
15	EIF3F	O00303	Eukaryotic translation initiation factor 3 subunit F	translational protein
16	EIF3H	O15372	Eukaryotic translation initiation factor 3 subunit H	translational protein

17	EIF3L	Q9Y262	Eukaryotic translation initiation factor 3 subunit L	translational protein
18	FLNA	P21333	Filamin-A	Unclassified
19	GOLM1	Q8NBJ4	Golgi membrane protein 1	Unclassified
20	GPI	P06744	Glucose-6-phosphate isomerase	metabolite interconversion enzyme
21	GSTM3	P21266	Glutathione S-transferase Mu 3	metabolite interconversion enzyme
22	HEXB	P07686	Beta-hexosaminidase subunit beta	metabolite interconversion enzyme
23	HSPA1L	P34931	Heat shock 70 kDa protein 1-like	chaperone
24	IQGAP1	P46940	Ras GTPase-activating-like protein IQGAP1	protein-binding activity modulator
25	ITIH2	P19823	Inter-alpha-trypsin inhibitor heavy chain H2	protein-binding activity modulator
26	P4HB	P07237	Protein disulfide-isomerase	chaperone
27	PAICS	P22234	Multifunctional protein ADE2 s	Unclassified
28	PRDX2	P32119	Peroxiredoxin-2	metabolite interconversion enzyme
29	PRDX6	P30041	Peroxiredoxin-6	Metabolite interconversion enzyme
30	PSMA4	P25789	Proteasome subunit alpha type 4	protein modifying enzyme
31	PSMB1	P20618	Proteasome subunit beta type 1	protein modifying enzyme
32	PSMB6	P28072	Proteasome subunit beta type 6	protein modifying enzyme
33	PSMC2	P35998	26S proteasome regulatory subunit 7	protein modifying enzyme
34	PSMC4	P43686	26S proteasome regulatory subunit 6B	protein modifying enzyme

35	PSMC5	P62195	26S proteasome regulatory subunit 8	protein modifying enzyme
36	PSMC6	P62333	26S proteasome regulatory subunit 10B	protein modifying enzyme
37	PSMD2	Q13200	26S proteasome non-ATPase regulatory subunit 2	protein modifying enzyme
38	PSMD3	O43242	26S proteasome non-ATPase regulatory subunit 3	protein modifying enzyme
39	RAN	P62826	GTP-binding nuclear protein Ran sapiens	protein-binding activity modulator
40	RPS15A	P62244	40S ribosomal protein S15a	translational protein
41	RUVBL1	Q9Y265	RuvB-like 1	Unclassified
42	RUVBL2	Q9Y230	RuvB-like 2	Unclassified
43	SFN	P31947	14-3-3 protein sigma	RNA metabolism protein
44	TOM1L1	O75874	Isocitrate dehydrogenase [NADP] cytoplasmic	Unclassified
45	TPI1	P60174	Triosephosphate isomerase	metabolite interconversion enzyme
46	TSPAN15	O95858	Tetraspanin-15	scaffold/adaptor protein
47	TUBA1C	Q9BQE3	Tubulin alpha-1C chain	cytoskeletal protein
48	VCL	P18206	Vinculin	Unclassified
49	YWHAB	P31946	14-3-3 protein beta/alpha	scaffold/adaptor protein

Finally, we use a Contaminant Repository for Affinity Purification (CRAPome) database (116). This resource contains negative control experiments generated by researchers around the world (raw mass spectrometry data) and the average of total spectra for each protein is calculated. We compared the average spectra of 69 and 49 specific cellular proteins in our virus and exosome fractions to the average spectrum of each protein in the CRAPome. We eliminated proteins that had less than a 2-fold increase in their average spectra compared to the negative control, which limits our results to 41 cellular proteins of interest in both virus and exosome fractions. The CRAPome data was next analyzed with PANTHER and IPA Ingenuity Pathway Analysis software. This narrowed down our targets to 14 and 5 cellular proteins of interest in the virus and exosome fractions respectively. Final cellular proteins of interest and the pathways they are involved in are summarized in Tables 6 and 7.

Table 6. Cellular proteins of interest and their pathways in the virus fraction

RNA metabolism	Metabolite interconversion enzymes	Protein modifying enzymes	Vesicular transport
MOV10	BPNT2(IMPAD)	SCYL1	RAB7A
PABPC1	MFGE8	TINAGL1	RAB2A
DDX1		PPP1CB	RAB6A
PABPC4		PRSS2	
SYNCRIP			

Table 7. Cellular proteins of interest and their pathways in the exosome fraction

Translational proteins	Metabolite interconversion enzymes	scaffold/adaptor protein
EIF3C	GSTM3	TSPAN15
DARS1		
CLU		

3.8 DsiRNA Knock-down

We hypothesized that the host proteins that are incorporated in to extracellular viruses play an important role in virus life cycle and propagation. Thus, we expected that by knocking down these proteins using RNA interference we would be able to identify the cellular proteins with an impact on virus titer. As a result, a total of 19 dsiRNAs (Dicer-Substrate Short Interfering RNAs) were designed to knock down cellular proteins, 14 of these targets found specifically in the virus fraction and 5 in the exosome fraction.

First, we checked the efficacy of our transfection protocol, using a fluorescent transfection control called "SiGLO" under the exact same conditions as dsiRNA-transfected-infected cells. HRT-18 cells were positively transfected with SiGLO compared to NC1, 72 hours post-transfection (Figure24A).

Next, we tested the cytotoxicity of the dsiRNA reagents using the AlamarBlue viability test. In our preliminary results, we found that for 16 targets, more than 90% of the cells were viable and active after dsiRNA knock-down compared to NC1 (a negative control dsiRNA that does not recognize human sequences). Moreover, cells transfected with other three targets showed a viability higher than 72% (Figure 24B). In summary, for all 19 targets the cells viability was more than 72%. Finally, since the cells were healthy and active after knocking-down the above host proteins, we monitored the effect of dsiRNA knock-down on HCoV-OC43 titration using $TCID_{50}$/ml-IPA. According to preliminary titration results (n=1), knocking down 13 targets reduced the HCoV-OC43 titer more than 50% compared to NC1, and knocking down one protein increased the viral titer more than two-fold (GSTM3) (Figure 24C). If reproducible, this would demonstrate the importance of these host proteins for productive virus propagation.

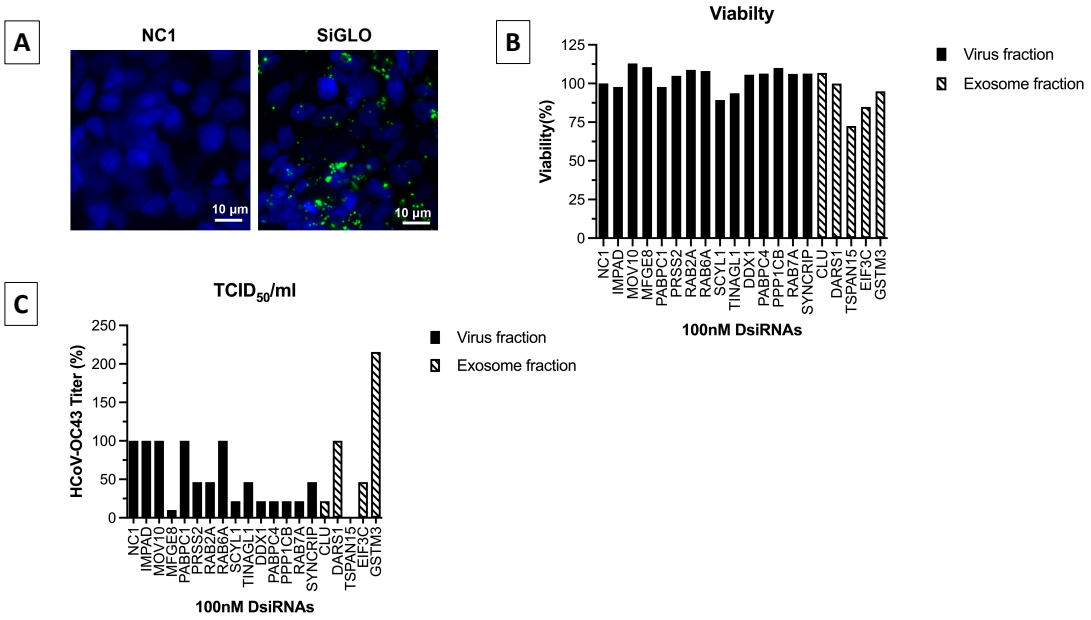

Figure 24. Effects of dsiRNAs on reduction of HCoV-OC43 production

A: SiGLO green, fluorescent signal was checked under Leica DMi8 inverted wide-field fluorescence microscope 72h post-transfection ***B:*** *HRT-18 cells viability was checked using 10% alamarBlue 72h post-transfection with 100nM dsiRNAs. The black bars represented the dsiRNAs targeted the virus fraction host proteins; striped bars show the dsiRNAs targeted the exosome fraction host proteins. Viability percentage for each target compared to NC1 (n=1)* ***C:*** *HRT-18 cells transfected with 100 nM dsiRNAs, 24h post-transfection cells were infected with HCoV-OC43 MOI 0.1 for 48 hrs, then the whole cell lysate was collected followed by virus titration using* $TCID_{50}$*/ml-IPA (n=1).* (n=1).

3.9 SARS-CoV-2

We have optimized the purification of HCoV-OC43 virions, separating them from exosomes, and characterized their unique cellular protein compositions. We next sought to analyze the more virulent SARS-CoV-2 virions using the same proteomic pipeline to gain a deeper understanding of beta Coronaviruses. Initially, our collaborators in Nathalie Grandvaux's laboratory prepared inactivated SARS-CoV-2 extracellular viruses. To this end, the titer of Delta SARS-CoV-2 released in the media of Vero-E6 infected cells was calculated by $TCID_{50}$ prior to inactivation with 0.05% β-Propiolactone for 16h at 4°C followed by 2h at 37°C and the titer was 1.04 x 10^8 pfu/mL. After inactivation the titer was re-evaluated, and no viable virus was detected. Back in our lab, we then concentrated the virus using Amicon 100 kDa filters followed by Optiprep density gradient ultracentrifugation as for HCoV-OC43. Our preliminary results showed that we could detect the SARS-CoV-2 S protein only in fractions 14 to 17 (Figure 23). However, we could not detect any of tetraspanin exosome markers CD9-CD63 and CD81 in any of the fractions, in agreement with our past findings that we could not detect the exosomes markers in the tissue culture media even after centrifugation at 100,000 *x g* (Figure 15). It will likely thus not be possible to analyse the protein content of exosomes in these cells.

Figure 25. SARS-CoV-2 fractionation

Inactivated extracellular SARS-CoV-2 samples were concentrated using 100 kDa Amicon Millipore filters. The samples were then loaded on top of a continuous Optiprep/sucrose gradient ranging from 8 to 25%, ultracentrifuged for 135 min at 250,000 × g at 4° C. Eighteen fractions were collected from the top (fraction 1) to the

bottom (fraction 18) of the gradient using a hydraulic pump. Fifty µl of each fraction were next loaded on a 5–20% gradient SDS gel. The separation of exosome markers and virus in each fraction was checked using antibodies against exosome markers CD9, CD63, CD81 and the S protein of SARS-CoV-2 (n=1 for the WB so far, but three viral purifications have already been done).

Chapter 4—Discussion

In our lab, we have previously studied the host proteins incorporated into extracellular viruses or purified HSV-1 nuclear capsids using MS (108, 117). MS-based proteomics is a powerful tool for studying virus-host interactions. Analyzing the proteomic profiles of the host proteins incorporated in purified viruses makes it possible for us to identify and characterize the host proteins that have an impact on different parts of the virus life cycle from replication, egress, and evading the immune system.

The covid-19 pandemic shifted the attention of scientists around the world to study coronaviruses, especially SARS-CoV-2. SARS-CoV-2 for now is classified as a Risk Group 3 (RG3) human pathogen that requires biosafety level 3 facilities for manipulation and studying the virus. During the pandemic, the American Society for Testing and Materials ASTM (118) expressed the importance of finding a surrogate for SARS-CoV-2 for method development. Although the entry route of SARS-CoV-2 and the cellular machinery that the virus uses to enter is different from HCoV-OC43, the endemic beta coronavirus HCoV-OC43 is an interesting surrogate as both viruses share common similarities during the virus life cycle and are part of the same subfamily of β coronaviruses. Moreover, the HCoV-OC43 is classified as a risk group 2 virus, which allows us to study this virus in level 2 biosafety facilities, which is more accessible than the biosafety level 3. Pharmacological inhibition studies on cellular pathways like endosome maturation, phosphatidylinositol phosphate biosynthesis, and cholesterol homeostasis show that the inhibition of these pathways will attenuate both HCoV-OC43 and SARS-CoV-2 propagation (119). Moreover, knock-out studies on ER membrane remodeling molecules show the importance of these molecules in the infectivity of both HCoV-OC43 and SARS-CoV-2 (120). These results validate the utility of HCoV-OC43 as a surrogate to study high-risk SARS-CoVs (21, 119). We consequently designed this project to first study the cellular proteins that are associated with highly purified extracellular HCoV-OC43 virus using MS with the optic to extend such studies to the more virulent SARS-CoV-2.

To study the proteome of HCoV-OC43, the purification of viruses from cellular protein contaminants was an important step. We know that mass spectrometers pick up contaminants and critical proteins indiscriminately. Keratin, cytoskeletal proteins, and the numerous proteins present in serum are common contaminants. Besides, high levels of these abundance proteins (for example BSA and immunoglobulins) can have adverse downstream effects, such as masking low abundance proteins. Besides protein contaminants, one also needs to consider exosomes. Exosomes are extracellular vesicles originating from cellular membranes. Exosomes carry cellular components like proteins, lipids, DNAs, and RNAs to other cells as a communication system between cells. During a viral infection, the exosome can carry viral proteins and genome as well. We therefore needed to separate the exosomes from extracellular viruses to have a more accurate MS analysis.

One of our strategies to reduce serum and exosome contaminants was to use OptiPRO, a serum-free media that eases downstream purification steps because Optipro, unlike serum, has an ultra-low protein concentration (7.5 µg/mL (121)). This enables us to collect purified extracellular medium with less protein contaminant. We used a 100kDa cut-off filter which concentrates all particles larger than 100kDa which are most of the exosomes and viruses. To get rid of the remaining exosomes in the samples, and separate them from viral particles, we next used the Optiprep density gradient. This technique allowed us to separate exosomes from infectious particles due to their different densities. In a study done by Dogrammatzis and collogues (109), they implemented the Optiprep density gradient technique to separate the distinct populations of extracellular vesicles released from HSV-1 infected cells. In other studies, the Optiprep density gradient ultracentrifugation was used as a successful technique in the separation of different populations of extracellular vesicles from Zika virus-infected cells (122), Epstein–Barr virus (123) and simian immunodeficiency virus-infected cells (124) to study the protein content of the extracellular vesicles and the impact of these proteins on virus infection.

4.1 Analysis of Virus and Exosome Fractions

WB and MS results indicate that HRT-18 cells only secrete CD9-CD63 positive exosomes. Furthermore, there is no evidence for larger exocytic vesicles based on our EM findings. Our WB, silver staining and EM data show that we have a very strong enrichment of infectious HCoV-OC43 particles with only traces of exosomes markers in the fraction but no exosomes per se. This indicates our purification protocol meets the purify requirements for MS. Although the exosome fraction produced by infected cells contained traces of the N viral protein by WB and infectious HCoV-OC43 particles by $TCID_{50}$/ml, that fraction contained 2 log fewer viral particles than virus fraction. Moreover, our MS results confirmed the enrichment of viral structural proteins in the virus fraction compared to the exosome fraction (Table 3). This enabled us to additionally probe the exosome content and alterations during the infection. While the HCOV-OC43 infection does not have an impact on the protein level and secretion of exosomes markers, it clearly impacts the composition of these vesicles, as our MS analysis shows 79 unique host proteins in exosomes produced by mock-infected cells vs 49 unique host proteins in HCoV-OC43 infected fraction 6. Oddly, our preliminary results on SARS-CoV-2 samples did not detect any exosome markers on the density gradients, perhaps a sign that Vero-E6 cells do not secrete appreciable amount of these vesicles. This is in agreement with our initial analysis prior to fractionation of the gradients.

4.2 Analysis of MS Results for HCoV-OC43 Virions

Up to now, there has been no study on the proteome of extracellular HCoV-OC43 virions. We filled that important void by probing the protein content of highly purified virions. Interestingly, many of the virion specific host proteins are associated with protein modification enzymes, vesicle trafficking proteins, and RNA metabolism enzymes such as RNA helicases. We also validated the relevance of these proteins for the virus by RNAi interference. Our preliminary results on knocking down these host targets using dsiRNAs, revealed that the virus titer decreased by at least 50% when knocking down the MFGE8, PRSS2, RAB2A, SCYL1, TINAGL1, DDX1, PABPC4, PPP1CB, RAB7A, SYNCRIP, CLU, TSPAN15, EIF3C host proteins. While these data must still be reproduced, all the protein modifying enzymes incorporated in the virions (SCYL1, TINAGL1, PPP1CB, PRSS2) had some impact on HCoV-OC43 production. These proteins are responsible for

post-translation modifications. For example, SCYL1 is a kinase and knockdown of SCYL1 disrupts the retrograde traffic between the Golgi and ER (125) moreover. Mutations of SCYL1 in mice results in motor neuron degeneration as well as cerebellar atrophy (126). PPP1CB is a serine/threonine phosphatase that interacts with the SARS-CoV-2 non-structural proteins nsp8, nsp10, nsp13 and orf9b (127). Our results indicate that the knocking down the SCYL1 and PPP1CB by RNA interference leads to reduction of infectious HCoV-OC43 particle production by 79%, although the exact impact and mechanism underlying this reduction is not yet known for HCoV-OC43.

Three of the 5 proteins modulating RNA metabolism family also appeared to have an impact on HCoV-OC43 replication. These proteins DDX1, PABPC4 and SYNCRIP are responsible for the modification, degradation, synthesis and folding of newly synthesized RNAs. Past MS studies suggest that the interaction between the SARS-CoV-2 N protein as well the 3' viral UTR with SYNCRIP promotes the replication and translation of the virus (129, 130). Additionally, DDX1 is an ATP-dependent RNA helicase and there is evidence that the association between DDX1 and Nsp14 may play a role in the replication of the infectious bronchitis virus coronavirus (131). Keeping in line with our results, knocking down both of these RNA modifying enzymes reduced the HCoV-OC43 titer.

Following the knock-down of the transport proteins Rab2a and Rab7a, we again observed a reduction in HCoV-OC43 titers, but interestingly not when targeting Rab6a, suggesting a specific interaction of the virus with select Rab proteins. Rab GTPases are crucial for modulating cellular trafficking pathways. Enveloped viruses like Coronaviruses take advantage of host vesicular trafficking machinery to complete their life cycle and propagation (128). The Rab GTPase like Rab2A and Rab7A were indeed found to be critical for HCoV-229E, HCoV-OC43, and HCoV-NL63 infection, but not SARS-CoV-2 (129).

Metabolite interconversion enzymes are family of enzymes which have hydrolase, transferases, or oxidoreductase activities. Our $TCID_{50}$ results showed that knocking down the metabolite interconversion enzyme MFGE8 reduced HCoV-OC43 titers by 90%. It has been suggested that MFGE8 is one of the SARS-CoV-2 ORF-8 interactor and it is predicted to increase the risk of acute

respiratory distress syndrome (130). In summary, from the 14 host proteins incorporated in HCoV-OC43 particles in the virus fraction, 10 proteins (71%) appear to play a crucial role in HCoV-OC43 replication and life cycle, and knocking down these proteins reduces virus production by more than 50%.

4.3 Analysis of MS results for HCoV-OC43 infected exosomes

Based on our MS results of the exosome fraction isolated from the supernatant of cells infected with HCoV-OC43, we observed numerous proteins associated with protein modifying enzymes, translational protein pathway and scaffold proteins. Preliminary results of the five targets that were chosen for RNA interference studies revealed that four of these host proteins have an impact on HCoV-OC43 production. Interestingly, EIF3C is an eukaryotic translation initiation factor. A study suggests that the increase of EIF3C protein in hepatocellular carcinoma is associated with tumor progression, increase level of exosomes and poor prognosis (131). We found a reduction in virus titers after knocking down the EIF3C, but for now, we do not know the impact of this knock down on exosome production. Similarly, our preliminary $TCID_{50}$ results suggest that knocking down TSPAN15 reduced the virus titer by 99.8% . TSPAN15 belongs to the tetraspanin superfamily of proteins, which is required for protein intracellular trafficking such as ADAM10 (132). ADAM10 is a proteolytic enzyme which cleaves the extracellular region of proteins such as Notch, amyloid precursor protein. It is suggested that dysregulation of this enzyme and mutations affecting ADAM10's enzymatic activity increase the risk of disorders such Alzheimer's disease (133). It is interesting to note that GSTM3, which is a metabolite interconversion enzyme, is the only host protein that when knocked down results in an increase of over 2 times in the HCoV-OC43 titer. GSTM3 is Members of the glutathione S-transferase (GST) superfamily, which are known for detoxifying oxidants and carcinogens (134). Studies show that GSTM3 overexpression is correlated with lymph node metastasis in colon cancer (135), while knocking down the GSTM1 and GSTM3 proteins significantly reduces tumor progression in cervical cancer (136). In contrast pancreatic cancer studies show that the overexpression of GSTM3 may suppress tumor growth by stopping the G0/G1 phase of the cell cycle (137). A possible

explanation for the rise in $TCID_{50}$ titration could thus be that GSTM3's inhibition of the cell cycle negatively impact virus production so depleting that protein favors the virus.

4.4 SARS-CoV-2 Virions

There have been studies on the proteome of SARS-CoV-2, but they have examined the interactions between SARS-CoV-2 structural and non-structural proteins with cellular proteins (138) or the host-pathogen interactions by yeast two-hybrid experiments (139). However, we plan to examine the whole proteome of purified extracellular virions produced by Vero-E6 cells, which has not been done to date. Additionally, we need to repeat these experiments, and then pursue the MS analysis of the purified viruses. Much of the present work focuses on HCoV-OC43. However, preliminary results are presented for SARS-CoV-2. Overall, we found that the protocol used to purify the virions is working for both viruses, so we could next proceed with our MS analysis.

Chapter 5—Conclusion

Viruses replicate and create new progeny by hijacking the host machinery. Studying Coronaviruses and finding new therapeutic targets have become increasingly important in the wake of the SARS-CoV-2 pandemic. HCoV-OC43, as a low-risk human coronavirus, is an opportunity to study the coronaviruses as both viruses share common life cycles.

We designed this study to investigate the proteome of the highly enriched extracellular HCoV-OC43 virus and find the host proteins incorporated in the virus. We have successfully established a protocol to obtain highly enriched HCoV-OC43 extracellular virions and separated the concentrated HCOV-OC43 virions from exosomes using density gradient fractionation. MS results confirm the enrichment of viral particles in the viral fraction, and 14 and 5 high-confidence host proteins were uniquely identified in the virus and exosome fractions (compared to the mock-infected controls). The knockdown of these 19 host targets appeared to affect virus production, although we still need to repeat these experiments. Moreover, we are now ready to expand our purification and separation protocol to study the proteome of SARS-CoV-2 virions as well.

In conclusion, studying the effect of the host proteins during viral replication and egress using knock-down studies can ultimately result in the identification of potential new targets for antiviral interventions. Moreover, by expanding our concentration and purification techniques to the SARS-CoV-2 virus, we will be able to compare the proteomes of these two β-coronaviruses. As a result, we will be able to gain a deeper insight into host-virus protein interactions and the role that they play in virus propagation.

References

1. Ambali A, Jones R. Early pathogenesis in chicks of infection with an enterotropic strain of infectious bronchitis virus. Avian Diseases. 1990:809-17.
2. Schalk AF, Hawn MC. An Apparently New Respiratory Disease of Baby Chicks. American Veterinary Medical Association. 1931;78:413-23.
3. Pagani I, Ghezzi S, Alberti S, Poli G, Vicenzi E. Origin and evolution of SARS-CoV-2. The European Physical Journal Plus. 2023;138(2):157.
4. van der Hoek L, Pyrc K, Jebbink MF, Vermeulen-Oost W, Berkhout RJM, Wolthers KC, et al. Identification of a new human coronavirus. Nature Medicine. 2004;10(4):368-73.
5. Kesheh MM, Hosseini P, Soltani S, Zandi M. An overview on the seven pathogenic human coronaviruses. Reviews in Medical Virology. 2022;32(2):e2282.
6. Wölfel R, Corman VM, Guggemos W, Seilmaier M, Zange S, Müller MA, et al. Virological assessment of hospitalized patients with COVID-2019. Nature. 2020;581(7809):465-9.
7. van Regenmortel MH, Fauquet CM, Bishop DH, Carstens E, Estes M, Lemon S, et al. Virus taxonomy: classification and nomenclature of viruses. Seventh report of the International Committee on Taxonomy of Viruses: Academic Press; 2000.
8. Masters PS. The molecular biology of coronaviruses. Advances in virus research. 2006;66:193-292.
9. Cui J, Li F, Shi Z-L. Origin and evolution of pathogenic coronaviruses. Nature Reviews Microbiology. 2019;17(3):181-92.
10. Cimolai N. Complicating infections associated with common endemic human respiratory coronaviruses. Health security. 2021;19(2):195-208.
11. Su S, Wong G, Shi W, Liu J, Lai AC, Zhou J, et al. Epidemiology, genetic recombination, and pathogenesis of coronaviruses. Trends in microbiology. 2016;24(6):490-502.
12. Tang G, Liu Z, Chen D. Human coronaviruses: Origin, host and receptor. Journal of Clinical Virology. 2022:105246.

13. El-Sahly HM, Atmar RL, Glezen WP, Greenberg SB. Spectrum of clinical illness in hospitalized patients with “common cold” virus infections. Clinical infectious diseases. 2000;31(1):96-100.

14. Ahsan MA, Liu Y, Feng C, Hofestädt R, Chen M. OverCOVID: an integrative web portal for SARS-CoV-2 bioinformatics resources. Journal of integrative bioinformatics. 2021;18(1):9-17.

15. Ogimi C, Kim YJ, Martin ET, Huh HJ, Chiu C-H, Englund JA. What’s new with the old coronaviruses? Journal of the Pediatric Infectious Diseases Society. 2020;9(2):210-7.

16. Jean A, Quach C, Yung A, Semret M. Severity and outcome associated with human coronavirus OC43 infections among children. The Pediatric infectious disease journal. 2013;32(4):325-9.

17. Vijgen L, Keyaerts E, Moës E, Thoelen I, Wollants E, Lemey P, et al. Complete genomic sequence of human coronavirus OC43: molecular clock analysis suggests a relatively recent zoonotic coronavirus transmission event. Journal of virology. 2005;79(3):1595-604.

18. Murray RS, Brown B, Brain D, Cabirac GF. Detection of coronavirus RNA and antigen in multiple sclerosis brain. Annals of Neurology: Official Journal of the American Neurological Association and the Child Neurology Society. 1992;31(5):525-33.

19. Jacomy H, Fragoso G, Almazan G, Mushynski WE, Talbot PJ. Human coronavirus OC43 infection induces chronic encephalitis leading to disabilities in BALB/C mice. Virology. 2006;349(2):335-46.

20. Luo X, Zhou G-Z, Zhang Y, Peng L-H, Zou L-P, Yang Y-S. Coronaviruses and gastrointestinal diseases. Military Medical Research. 2020;7:1-6.

21. Kim MI, Lee C. Human Coronavirus OC43 as a Low-Risk Model to Study COVID-19. Viruses. 2023;15(2):578.

22. Desforges M, Le Coupanec A, Dubeau P, Bourgouin A, Lajoie L, Dubé M, et al. Human coronaviruses and other respiratory viruses: underestimated opportunistic pathogens of the central nervous system? viruses. 2019;12(1):14.

23. Santerre M, Arjona SP, Allen CNS, Shcherbik N, Sawaya BE. Why do SARS-CoV-2 NSPs rush to the ER? Journal of Neurology. 2021;268(6):2013-22.

24. Guo Y, Korteweg C, McNutt MA, Gu J. Pathogenetic mechanisms of severe acute respiratory syndrome. Virus research. 2008;133(1):4-12.

25. Li Y-C, Bai W-Z, Hirano N, Hayashida T, Hashikawa T. Coronavirus infection of rat dorsal root ganglia: ultrastructural characterization of viral replication, transfer, and the early response of satellite cells. Virus research. 2012;163(2):628-35.

26. Netland J, Meyerholz DK, Moore S, Cassell M, Perlman S. Severe acute respiratory syndrome coronavirus infection causes neuronal death in the absence of encephalitis in mice transgenic for human ACE2. Journal of virology. 2008;82(15):7264-75.

27. Li YC, Bai WZ, Hirano N, Hayashida T, Taniguchi T, Sugita Y, et al. Neurotropic virus tracing suggests a membranous-coating-mediated mechanism for transsynaptic communication. Journal of Comparative Neurology. 2013;521(1):203-12.

28. Matsuda K, Park C, Sunden Y, Kimura T, Ochiai K, Kida H, et al. The vagus nerve is one route of transneural invasion for intranasally inoculated influenza a virus in mice. Veterinary pathology. 2004;41(2):101-7.

29. Marzi M, Vakil MK, Bahmanyar M, Zarenezhad E. Paxlovid: Mechanism of Action, Synthesis, and In Silico Study. BioMed Research International. 2022;2022:7341493.

30. Umemura T, Mutoh Y, Mizuno T, Hagihara M, Kato H, Yamada T, et al., editors. Safety Evaluation of Remdesivir for COVID-19 Patients with eGFR< 30 mL/min without Renal Replacement Therapy in a Japanese Single-Center Study. Healthcare; 2022: MDPI.

31. Canada H. COVID-19 vaccines and treatments portal 2023 [Available from: https://covid-vaccine.canada.ca/.

32. Basu D, Chavda VP, Mehta AA. Therapeutics for COVID-19 and post COVID-19 complications: An update. Current Research in Pharmacology and Drug Discovery. 2022;3:100086.

33. Rappe JCF, de Wilde A, Di H, Müller C, Stalder H, V'kovski P, et al. Antiviral activity of K22 against members of the order Nidovirales. Virus research. 2018;246:28-34.

34. Koppers-Lalic D, Hogenboom MM, Middeldorp JM, Pegtel DM. Virus-modified exosomes for targeted RNA delivery; a new approach in nanomedicine. Advanced drug delivery reviews. 2013;65(3):348-56.

35. Saad MH, Badierah R, Redwan EM, El-Fakharany EM. A Comprehensive Insight into the Role of Exosomes in Viral Infection: Dual Faces Bearing Different Functions. Pharmaceutics. 2021;13(9):1405.

36. El-Shennawy L, Hoffmann AD, Dashzeveg NK, McAndrews KM, Mehl PJ, Cornish D, et al. Circulating ACE2-expressing extracellular vesicles block broad strains of SARS-CoV-2. Nature Communications. 2022;13(1):405.

37. Lan Q, Wang L, Jiao F, Lu L, Xia S, Jiang S. Pan-coronavirus fusion inhibitors to combat COVID-19 and other emerging coronavirus infectious diseases. Journal of Medical Virology. 2023;95(1):e28143.

38. Mingaleeva RN, Nigmatulina NA, Sharafetdinova LM, Romozanova AM, Gabdoulkhakova AG, Filina YV, et al. Biology of the SARS-CoV-2 Coronavirus. Biochemistry (Moscow). 2022;87(12):1662-78.

39. Liu DX, Liang JQ, Fung TS. Human coronavirus-229E,-OC43,-NL63, and-HKU1 (Coronaviridae). Encyclopedia of virology. 2021:428.

40. Desforges M, Desjardins J, Zhang C, Talbot PJ. The acetyl-esterase activity of the hemagglutinin-esterase protein of human coronavirus OC43 strongly enhances the production of infectious virus. Journal of virology. 2013;87(6):3097-107.

41. Bai Z, Cao Y, Liu W, Li J. The SARS-CoV-2 nucleocapsid protein and its role in viral structure, biological functions, and a potential target for drug or vaccine mitigation. Viruses. 2021;13(6):1115.

42. Chen J, Malone B, Llewellyn E, Grasso M, Shelton PM, Olinares PDB, et al. Structural basis for helicase-polymerase coupling in the SARS-CoV-2 replication-transcription complex. Cell. 2020;182(6):1560-73. e13.

43. Ziebuhr J, Snijder EJ, Gorbalenya AE. Virus-encoded proteinases and proteolytic processing in the Nidovirales. Journal of General Virology. 2000;81(4):853-79.

44. Chen B, Tian E-K, He B, Tian L, Han R, Wang S, et al. Overview of lethal human coronaviruses. Signal Transduction and Targeted Therapy. 2020;5(1):89.

45. Zmasek CM, Lefkowitz EJ, Niewiadomska A, Scheuermann RH. Genomic evolution of the Coronaviridae family. Virology. 2022;570:123-33.

46. V'kovski P, Kratzel A, Steiner S, Stalder H, Thiel V. Coronavirus biology and replication: implications for SARS-CoV-2. Nature Reviews Microbiology. 2021;19(3):155-70.

47. Liu DX, Liang JQ, Fung TS. Human Coronavirus-229E, -OC43, -NL63, and -HKU1 (Coronaviridae). In: Bamford DH, Zuckerman M, editors. Encyclopedia of Virology (Fourth Edition). Oxford: Academic Press; 2021. p. 428-40.

48. Wu A, Peng Y, Huang B, Ding X, Wang X, Niu P, et al. Genome composition and divergence of the novel coronavirus (2019-nCoV) originating in China. Cell host & microbe. 2020;27(3):325-8.

49. Rowan-Nash AD, Korry BJ, Mylonakis E, Belenky P. Cross-Domain and Viral Interactions in the Microbiome. Microbiology and Molecular Biology Reviews. 2019;83(1):e00044-18.

50. Beidas M, Chehadeh W. PCR array profiling of antiviral genes in human embryonic kidney cells expressing human coronavirus OC43 structural and accessory proteins. Archives of Virology. 2018;163(8):2065-72.

51. Beidas M, Chehadeh W. Effect of Human Coronavirus OC43 Structural and Accessory Proteins on the Transcriptional Activation of Antiviral Response Elements. Intervirology. 2018;61(1):30-5.

52. Hulswit RJ, Lang Y, Bakkers MJ, Li W, Li Z, Schouten A, et al. Human coronaviruses OC43 and HKU1 bind to 9-O-acetylated sialic acids via a conserved receptor-binding site in spike protein domain A. Proceedings of the National Academy of Sciences. 2019;116(7):2681-90.

53. Ren L, Zhang Y, Li J, Xiao Y, Zhang J, Wang Y, et al. Genetic drift of human coronavirus OC43 spike gene during adaptive evolution. Scientific Reports. 2015;5:11451.

54. Wang C, Hesketh EL, Shamorkina TM, Li W, Franken PJ, Drabek D, et al. Antigenic structure of the human coronavirus OC43 spike reveals exposed and occluded neutralizing epitopes. Nature Communications. 2022;13(1):2921.

55. Bakkers MJG, Lang Y, Feitsma LJ, Hulswit RJG, de Poot SAH, van Vliet ALW, et al. Betacoronavirus Adaptation to Humans Involved Progressive Loss of Hemagglutinin-Esterase Lectin Activity. Cell Host & Microbe. 2017;21(3):356-66.

56. Lang Y, Li W, Li Z, Koerhuis D, van den Burg ACS, Rozemuller E, et al. Coronavirus hemagglutinin-esterase and spike proteins coevolve for functional balance and optimal virion avidity. Proceedings of the National Academy of Sciences. 2020;117(41):25759-70.

57. Hasöksüz M, Kilic S, Sarac F. Coronaviruses and sars-cov-2. Turkish journal of medical sciences. 2020;50(9):549-56.

58. Stodola JK, Dubois G, Le Coupanec A, Desforges M, Talbot PJ. The OC43 human coronavirus envelope protein is critical for infectious virus production and propagation in neuronal cells and is a determinant of neurovirulence and CNS pathology. Virology. 2018;515:134-49.

59. Mounir S, Labonté P, Talbot PJ. Characterization of the Nonstructural and Spike Proteins of the Human Respiratory Coronavirus OC43: Comparison with Bovine Enteric Coronavirus. In: Laude H, Vautherot J-F, editors. Coronaviruses: Molecular Biology and Virus-Host Interactions. Boston, MA: Springer US; 1993. p. 61-7.

60. Vennema H, Godeke GJ, Rossen J, Voorhout WF, Horzinek MC, Opstelten D, et al. Nucleocapsid-independent assembly of coronavirus-like particles by co-expression of viral envelope protein genes. The EMBO journal. 1996;15(8):2020-8.

61. Fung TS, Liu DX. Human Coronavirus: Host-Pathogen Interaction. Annual Review of Microbiology. 2019;73(1):529-57.

62. Masters PS. The Molecular Biology of Coronaviruses. Advances in Virus Research. 66: Academic Press; 2006. p. 193-292.

63. Mu J, Xu J, Zhang L, Shu T, Wu D, Huang M, et al. SARS-CoV-2-encoded nucleocapsid protein acts as a viral suppressor of RNA interference in cells. Science China Life Sciences. 2020;63:1413-6.

64. Cubuk J, Alston JJ, Incicco JJ, Singh S, Stuchell-Brereton MD, Ward MD, et al. The SARS-CoV-2 nucleocapsid protein is dynamic, disordered, and phase separates with RNA. Nature communications. 2021;12(1):1936.

65. Iserman C, Roden C, Boerneke M, Sealfon R, McLaughlin G, Jungreis I, et al. Specific viral RNA drives the SARS CoV-2 nucleocapsid to phase separate. bioRxiv. 2020:2020.06.11.147199.

66. Huang C, Lokugamage KG, Rozovics JM, Narayanan K, Semler BL, Makino S. SARS coronavirus nsp1 protein induces template-dependent endonucleolytic cleavage of mRNAs: viral mRNAs are resistant to nsp1-induced RNA cleavage. PLoS pathogens. 2011;7(12):e1002433.

67. Gupta M, Azumaya CM, Moritz M, Pourmal S, Diallo A, Merz GE, et al. CryoEM and AI reveal a structure of SARS-CoV-2 Nsp2, a multifunctional protein involved in key host processes. Research square. 2021.

68. Thiel V, Ivanov KA, Putics Á, Hertzig T, Schelle B, Bayer S, et al. Mechanisms and enzymes involved in SARS coronavirus genome expression. Journal of General Virology. 2003;84(Pt 9):2305-15.

69. Sakai Y, Kawachi K, Terada Y, Omori H, Matsuura Y, Kamitani W. Two-amino acids change in the nsp4 of SARS coronavirus abolishes viral replication. Virology. 2017;510:165-74.

70. Te Velthuis AJ, Van Den Worm SH, Snijder EJ. The SARS-coronavirus nsp7+ nsp8 complex is a unique multimeric RNA polymerase capable of both de novo initiation and primer extension. Nucleic acids research. 2012;40(4):1737-47.

71. El-Kamand S, Du Plessis MD, Breen N, Johnson L, Beard S, Kwan AH, et al. A distinct ssDNA/RNA binding interface in the Nsp9 protein from SARS-CoV-2. Proteins: Structure, Function, and Bioinformatics. 2022;90(1):176-85.

72. Rona G, Zeke A, Miwatani-Minter B, de Vries M, Kaur R, Schinlever A, et al. The NSP14/NSP10 RNA repair complex as a Pan-coronavirus therapeutic target. Cell Death & Differentiation. 2022;29(2):285-92.

73. Jang K-J, Jeong S, Kang DY, Sp N, Yang YM, Kim D-E. A high ATP concentration enhances the cooperative translocation of the SARS coronavirus helicase nsP13 in the unwinding of duplex RNA. Scientific reports. 2020;10(1):1-13.

74. Yuen C-K, Lam J-Y, Wong W-M, Mak L-F, Wang X, Chu H, et al. SARS-CoV-2 nsp13, nsp14, nsp15 and orf6 function as potent interferon antagonists. Emerging microbes & infections. 2020;9(1):1418-28.

75. Decroly E, Debarnot C, Ferron F, Bouvet M, Coutard B, Imbert I, et al. Crystal structure and functional analysis of the SARS-coronavirus RNA cap 2'-O-methyltransferase nsp10/nsp16 complex. PLoS pathogens. 2011;7(5):e1002059.

76. Reusken CB, Raj VS, Koopmans MP, Haagmans BL. Cross host transmission in the emergence of MERS coronavirus. Current opinion in virology. 2016;16:55-62.

77. Collins AR. HLA class I antigen serves as a receptor for human coronavirus OC43. Immunological investigations. 1993;22(2):95-103.

78. Owczarek K, Szczepanski A, Milewska A, Baster Z, Rajfur Z, Sarna M, et al. Early events during human coronavirus OC43 entry to the cell. Scientific Reports. 2018;8(1):7124.

79. Lau SK, Lung DC, Wong EY, Aw-Yong KL, Wong AC, Luk HK, et al. Molecular evolution of human coronavirus 229E in Hong Kong and a fatal COVID-19 case involving coinfection with a novel human coronavirus 229E genogroup. MSphere. 2021;6(1):e00819-20.

80. Pizzato M, Baraldi C, Boscato Sopetto G, Finozzi D, Gentile C, Gentile MD, et al. SARS-CoV-2 and the Host Cell: A Tale of Interactions. Frontiers in Virology. 2022;1.

81. Perlman S, Netland J. Coronaviruses post-SARS: update on replication and pathogenesis. Nature reviews microbiology. 2009;7(6):439-50.

82. Knoops K, Kikkert M, Worm SHvd, Zevenhoven-Dobbe JC, Van Der Meer Y, Koster AJ, et al. SARS-coronavirus replication is supported by a reticulovesicular network of modified endoplasmic reticulum. PLoS biology. 2008;6(9):e226.

83. Sawicki SG, Sawicki DL. Coronaviruses use discontinuous extension for synthesis of subgenome-length negative strands. Corona-and related viruses: current concepts in molecular biology and pathogenesis. 1995:499-506.

84. Viehweger A, Krautwurst S, Lamkiewicz K, Madhugiri R, Ziebuhr J, Hölzer M, et al. Direct RNA nanopore sequencing of full-length coronavirus genomes provides novel insights into structural variants and enables modification analysis. Genome research. 2019;29(9):1545-54.

85. de Haan CA, Rottier PJ. Molecular interactions in the assembly of coronaviruses. Advances in virus research. 2005;64:165-230.

86. Bos EC, Luytjes W, Van Der Meulen H, Koerten HK, Spaan WJ. The production of recombinant infectious DI-particles of a murine coronavirus in the absence of helper virus. Virology. 1996;218(1):52-60.

87. Li S, Dong R, Kang Z, Li H, Wu X, Li T. Exosomes: Another intercellular lipometabolic communication mediators in digestive system neoplasms? Cytokine & Growth Factor Reviews. 2023;73:93-100.

88. Andreu Z, Yáñez-Mó M. Tetraspanins in extracellular vesicle formation and function. Frontiers in immunology. 2014;5:442.

89. Liu Y-J, Wang C. A review of the regulatory mechanisms of extracellular vesicles-mediated intercellular communication. Cell Communication and Signaling. 2023;21(1):77.

90. Kalluri R, LeBleu VS. The biology, function, and biomedical applications of exosomes. Science. 2020;367(6478):eaau6977.

91. Edgar JR. Q&A: What are exosomes, exactly? BMC Biology. 2016;14(1):46.

92. Krylova SV, Feng D. The Machinery of Exosomes: Biogenesis, Release, and Uptake. International Journal of Molecular Sciences. 2023;24(2):1337.

93. Bebelman MP, Smit MJ, Pegtel DM, Baglio SR. Biogenesis and function of extracellular vesicles in cancer. Pharmacology & Therapeutics. 2018;188:1-11.

94. van Niel G, D'Angelo G, Raposo G. Shedding light on the cell biology of extracellular vesicles. Nature Reviews Molecular Cell Biology. 2018;19(4):213-28.

95. Ni Z, Zhou S, Li S, Kuang L, Chen H, Luo X, et al. Exosomes: roles and therapeutic potential in osteoarthritis. Bone Research. 2020;8(1):25.

96. Kalluri R, LeBleu VS. The biology,function and biomedical applications of exosomes. Science. 2020;367(6478):eaau6977.

97. Dai J, Su Y, Zhong S, Cong L, Liu B, Yang J, et al. Exosomes: key players in cancer and potential therapeutic strategy. Signal Transduction and Targeted Therapy. 2020;5(1):145.

98. Campanella C, Bavisotto CC, Gammazza AM, Nikolic D, Rappa F, David S, et al. Exosomal heat shock proteins as new players in tumour cell-to-cell communication. Journal of Circulating Biomarkers. 2014;3(1).

99. Mulcahy LA, Pink RC, Carter DRF. Routes and mechanisms of extracellular vesicle uptake. Journal of extracellular vesicles. 2014;3(1):24641.

100. Chaudhari P, Ghate V, Nampoothiri M, Lewis S. Multifunctional role of exosomes in viral diseases: From transmission to diagnosis and therapy. Cellular Signalling. 2022;94:110325.

101. Peng Y, Yang Y, Li Y, Shi T, Luan Y, Yin C. Exosome and virus infection. Frontiers in Immunology. 2023;14.

102. Pesce E, Manfrini N, Cordiglieri C, Santi S, Bandera A, Gobbini A, et al. Exosomes Recovered From the Plasma of COVID-19 Patients Expose SARS-CoV-2 Spike-Derived Fragments and Contribute to the Adaptive Immune Response. Frontiers in Immunology. 2022;12.

103. Fernbach S, Hale BG. SARS-CoV-2 takes the bait: Exosomes as endogenous decoys. PLOS Biology. 2022;20(9):e3001787.

104. El-Shennawy L, Hoffmann AD, Dashzeveg NK, McAndrews KM, Mehl PJ, Cornish D, et al. Circulating ACE2-expressing extracellular vesicles block broad strains of SARS-CoV-2. Nature communications. 2022;13(1):405.

105. Zhou S, Liu R, Zhao X, Huang C, Wei Y. Viral proteomics: the emerging cutting-edge of virus research. Science China Life Sciences. 2011;54:502-12.

106. Zeng R, Ruan H-Q, Jiang X-S, Zhou H, Shi L, Zhang L, et al. Proteomic Analysis of SARS Associated Coronavirus Using Two-Dimensional Liquid Chromatography Mass Spectrometry and One-Dimensional Sodium Dodecyl Sulfate-Polyacrylamide Gel Electrophoresis Followed by Mass Spectroemtric Analysis. Journal of Proteome Research. 2004;3(3):549-55.

107. Hodge K, Ten Have S, Hutton L, Lamond AI. Cleaning up the masses: exclusion lists to reduce contamination with HPLC-MS/MS. Journal of proteomics. 2013;88:92-103.

108. Loret S, Guay G, Lippé R. Comprehensive characterization of extracellular herpes simplex virus type 1 virions. Journal of virology. 2008;82(17):8605-18.

109. Dogrammatzis C, Saleh S, Deighan C, Kalamvoki M. Diverse populations of extracellular vesicles with opposite functions during herpes simplex virus 1 infection. Journal of Virology. 2021;95(6):e02357-20.

110. Savoie C, Lippé R. Optimizing human coronavirus OC43 growth and titration. PeerJ. 2022;10:e13721.

111. Lei C, Yang J, Hu J, Sun X. On the calculation of TCID 50 for quantitation of virus infectivity. Virologica Sinica. 2021;36:141-4.

112. Ludwig N, Whiteside TL, Reichert TE. Challenges in Exosome Isolation and Analysis in Health and Disease. International Journal of Molecular Sciences. 2019;20(19):4684.

113. Alzhrani GN, Alanazi ST, Alsharif SY, Albalawi AM, Alsharif AA, Abdel-Maksoud MS, et al. Exosomes: Isolation, characterization, and biomedical applications. Cell Biology International. 2021;45(9):1807-31.

114. Hurdiss DL, Drulyte I, Lang Y, Shamorkina TM, Pronker MF, van Kuppeveld FJM, et al. Cryo-EM structure of coronavirus-HKU1 haemagglutinin esterase reveals architectural changes arising from prolonged circulation in humans. Nature Communications. 2020;11(1):4646.

115. Venkatagopalan P, Daskalova SM, Lopez LA, Dolezal KA, Hogue BG. Coronavirus envelope (E) protein remains at the site of assembly. Virology. 2015;478:75-85.

116. The Contaminant Repository for Affinity Purification (CRAPome) [Available from: https://reprint-apms.org/.

117. El Bilali N, Khadivjam B, Bonneil E, Thibault P, Lippé R. Proteomics of Herpes Simplex Virus 1 Nuclear Capsids. Journal of Virology. 2021;95(4):e01842-19.

118. Schirtzinger EE, Kim Y, Davis AS. Improving human coronavirus OC43 (HCoV-OC43) research comparability in studies using HCoV-OC43 as a surrogate for SARS-CoV-2. Journal of Virological Methods. 2022;299:114317.

119. Wang R, Simoneau CR, Kulsuptrakul J, Bouhaddou M, Travisano KA, Hayashi JM, et al. Genetic Screens Identify Host Factors for SARS-CoV-2 and Common Cold Coronaviruses. Cell. 2021;184(1):106-19.e14.

120. Schneider WM, Luna JM, Hoffmann HH, Sánchez-Rivera FJ, Leal AA, Ashbrook AW, et al. Genome-Scale Identification of SARS-CoV-2 and Pan-coronavirus Host Factor Networks. Cell. 2021;184(1):120-32.e14.

121. Inc GTFS. OptiPRO™ SFM.

122. Zhao F, Xu Y, Liu N, Lv D, Chen Y, Liu Z, et al. Extracellular vesicles from Zika virus-infected cells display viral E protein that binds ZIKV-neutralizing antibodies to prevent infection enhancement. The EMBO Journal. 2023;42(6):e112096.

123. Sato Y, Yaguchi M, Okuno Y, Ishimaru H, Sagou K, Ozaki S, et al. Epstein–Barr virus tegument protein BGLF2 in exosomes released from virus-producing cells facilitates de novo infection. Cell Communication and Signaling. 2022;20(1):95.

124. Huang Y, Liao Z, Dang P, Queen S, Abreu CM, Gololobova O, et al. Longitudinal characterization of circulating extracellular vesicles and small RNA during simian immunodeficiency virus infection and antiretroviral therapy. Aids. 2023;37(5):733-44.

125. Burman JL, Bourbonniere L, Philie J, Stroh T, Dejgaard SY, Presley JF, et al. Scyl1, Mutated in a Recessive Form of Spinocerebellar Neurodegeneration, Regulates COPI-mediated Retrograde Traffic. Journal of Biological Chemistry. 2008;283(33):22774-86.

126. Pelletier S, Gingras S, Howell S, Vogel P, Ihle JN. An early onset progressive motor neuron disorder in Scyl1-deficient mice is associated with mislocalization of TDP-43. Journal of Neuroscience. 2012;32(47):16560-73.

127. Otvos LP, Garrito GIM, Machado LESF. Potential involvement of protein phosphatase PP2CA on protein synthesis and cell cycle during SARS-CoV-2 infection. A meta analysis investigation. bioRxiv. 2023:2023.06.02.543487.

128. Spearman P. Viral interactions with host cell Rab GTPases. Small GTPases. 2018;9(1-2):192-201.

129. Hoffmann HH, Sánchez-Rivera FJ, Schneider WM, Luna JM, Soto-Feliciano YM, Ashbrook AW, et al. Functional interrogation of a SARS-CoV-2 host protein interactome identifies unique and shared coronavirus host factors. Cell Host & Microbe. 2021;29(2):267-80.e5.

130. Fahmi M, Kitagawa H, Yasui G, Kubota Y, Ito M. The Functional Classification of ORF8 in SARS-CoV-2 Replication, Immune Evasion, and Viral Pathogenesis Inferred through Phylogenetic Profiling. Evolutionary Bioinformatics. 2021;17:11769343211003079.

131. Li S, Chen L. Exosomes in Pathogenesis, Diagnosis, and Treatment of Hepatocellular Carcinoma. Frontiers in Oncology. 2022;12.

132. Koo CZ, Harrison N, Noy PJ, Szyroka J, Matthews AL, Hsia H-E, et al. The tetraspanin Tspan15 is an essential subunit of an ADAM10 scissor complex. Journal of Biological Chemistry. 2020;295(36):12822-39.

133. Jansen IE, Savage JE, Watanabe K, Bryois J, Williams DM, Steinberg S, et al. Genome-wide meta-analysis identifies new loci and functional pathways influencing Alzheimer's disease risk. Nature Genetics. 2019;51(3):404-13.

134. Wang S, Yang J, You L, Dai M, Zhao Y. GSTM3 Function and Polymorphism in Cancer: Emerging but Promising. Cancer Management and Research. 2020;12:10377-88.

135. Meding S, Balluff B, Elsner M, Schöne C, Rauser S, Nitsche U, et al. Tissue-based proteomics reveals FXYD3, S100A11 and GSTM3 as novel markers for regional lymph node metastasis in colon cancer. The Journal of pathology. 2012;228(4):459-70.

136. Checa-Rojas A, Delgadillo-Silva LF, Velasco-Herrera MdC, Andrade-Domínguez A, Gil J, Santillán O, et al. GSTM3 and GSTP1: novel players driving tumor progression in cervical cancer. Oncotarget. 2018;9(31).

137. Wang S, Yang J, Ding C, Li J, You L, Dai M, et al. Glutathione S-Transferase Mu-3 Predicts a Better Prognosis and Inhibits Malignant Behavior and Glycolysis in Pancreatic Cancer. Frontiers in Oncology. 2020;10.

138. Gordon DE, Jang GM, Bouhaddou M, Xu J, Obernier K, White KM, et al. A SARS-CoV-2 protein interaction map reveals targets for drug repurposing. Nature. 2020;583(7816):459-68.

139. Zhou Y, Liu Y, Gupta S, Paramo MI, Hou Y, Mao C, et al. A comprehensive SARS-CoV-2–human protein–protein interactome reveals COVID-19 pathobiology and potential host therapeutic targets. Nature Biotechnology. 2023;41(1):128-39.